ANALYSIS OF A Λ_b^0 DECAY MODE

By

María Magdalena Falla Solórzano

A thesis submitted in partial fulfillment of the requirements for the degree of

MASTER OF SCIENCE

in

PHYSICS

UNIVERSITY OF PUERTO RICO
MAYAGÜEZ CAMPUS

2013

Approved by:

Héctor Méndez-Mella, Ph.D. President, Graduate Committee	Date
Samuel A. Santana-Colón, Ph.D. Member, Graduate Committee	Date
Juan Eduardo Ramírez-Vargas, Ph.D. Member, Graduate Committee	Date
Héctor Carlo, Ph.D. Representative of Graduate Studies	Date
Dorial Castellanos-Rodríguez, Ph.D. Chairperson of the Department	Date

Abstract of Dissertation Presented to the Graduate School
of the University of Puerto Rico in Partial Fulfillment of the
Requirements for the Degree of Master of Science

ANALYSIS OF A Λ_b^0 DECAY MODE

By

María Magdalena Falla Solórzano

May 2013

Chair: Héctor Méndez-Mella
Major Department: Physics

This thesis presents a preliminary results for the first observation of the exclusive $\Lambda_b^0 \rightarrow \Lambda^0\psi(2S)$ decay with a significance of 7.8 σ. The data sample used in this work, corresponding to an integrated luminosity of approximately 5.3 fb^{-1}, was collected by the Compact Muon Solenoid (CMS) experiment at the Large Hadron Collider (LHC) in proton-proton collisions at $\sqrt{\mathbf{s}} = 7$ TeV. The preliminary relative branching fraction is measured with respect to the normalizing $\Lambda_b^0 \rightarrow \Lambda^0 J/\psi$ decay mode where the $\psi(2S)$ has been reconstructed in the $\psi(2S) \rightarrow \mu^+\mu^-$ decay mode, the $\Lambda^0 \rightarrow p\pi^-$ final state and the J/ψ in the $\mu^+\mu^-$. The B($\Lambda_b^0 \rightarrow \Lambda^0\psi(2S)$)/B($\Lambda_b^0 \rightarrow \Lambda^0 J/\psi$) has been measured to be 0.66 $\pm$0.11(stat) $\pm$0.07(syst) $\pm$0.07(PDG), where the second and third terms are the statistical and systematic uncertainties and the PDG uncertainty term is due to the J/ψ/$\psi(2S)$ relative branching fraction in the dimuon channel. This result is still under review by the CMS collaboration and it is not an official result yet.

Resumen de Disertación Presentado a la Escuela Graduada
de la Universidad de Puerto Rico como requisito parcial de los
Requerimientos para el grado de Maestría en Ciencias

ANÁLISIS DE UN MODO DE DECAIMIENTO DE Λ_b^0

Por

María Magdalena Falla Solórzano

May 2013

Consejero: Héctor Méndez-Mella
Departamento: Física

En esta tesis se presentan los resultados preliminares de la primera observación del decaimiento exclusivo $\Lambda_b^0 \to \Lambda^0 \psi(2S)$ con una significancia de 7.8 σ. La muestra utilizada en este trabajo, corresponde a una luminosidad integrada de aproximadamente 5.3 fb^{-1}, y fue colectada por el experimento "Solenoide Compacto de Muones" (CMS) en el "Gran Colisionador de Hadrones" (LHC) en colisiones protón protón con una energía del centro de masa de $\sqrt{\mathbf{s}} =$ 7 TeV. La medida preliminar del "branching fraction " relativo se hace con respecto al modo de decaimiento $\Lambda_b^0 \to \Lambda^0 J/\psi$ (modo de normalización) donde la partícula $\psi(2S)$ ha sido reconstruida en el modo de decaimiento $\psi(2S) \to \mu^+\mu^-$, $\Lambda^0 \to p\pi^-$ y J/ψ en $\mu^+\mu^-$. El valor del "branching fraction " relativo B($\Lambda_b^0 \to \Lambda^0 \psi(2S)$)/B($\Lambda_b^0 \to \Lambda^0 J/\psi$) preliminarmente obtenido es 0.66 $\pm$0.11(stat) $\pm$0.07(syst) $\pm$0.07(PDG), donde el segundo y tercer termino son las incertidumbres estadisticas y sistematicas y el término PDG de la incertidumbre es debido al "branching fraction " de J/ψ/$\psi(2S)$ en el canal dimuonico. Este resultado sigue en proceso de revisión por la colaboración CMS y no es un resultado oficial aún.

ACKNOWLEDGMENTS

This thesis is the result of hard work of the group of high energy physics in the University of Puerto Rico.

Specially I want to give a sincere acknowledgement to:

- To all my family because always they bring me their love and support to undertake my goals.
- Dr. Héctor Méndez for his great guidance and support.
- Dr. Ángel López for the opportunity to work in the High Energy Physics Group of the University of Puerto Rico - Mayagüez Campus.
- Dr. Eduardo Ramirez and Dr. Samuel Santana for their participation at the committee.

Contents

List of Tables

Table page

List of Figures

Figure page

Chapter 1
INTRODUCTION

Present-day particle physics is a branch of physics extensively studied, and represents man's most ambicious and organized effort to answer the question: What is the world made of? The answer to this question was extracted step by step from a series of experiments embracing the fields of atomic, nuclear, cosmic-ray, and high-energy physics. The experimental effort was a sequence of very important discoveries in the last decade that directly guided us to a world of different particles [1]. The traditional goal of particle physics has been to identify what appears to be structureless units of matter and to understand the nature of the forces acting between them [2].

A theoretical framework was needed that could translate these conceptual developments into a quantitative calculational scheme. In the early 1930s, a theory emerged describing the electromagnetic interactions of electrons and photons (quantum electrodynamics) and conforming the desired theoretical framework. Even though it has become essential to include quarks, as well as leptons, and to consider other interactions besides electromagnetism, relativistic quantum field theory stands unchanged as the calculational framework of particle physics. The most recent developments in particle physics, however, have revealed the relevance of a special class of such theories, called "gauge" theories. The weak and strong interactions of quarks and leptons are believed to be described by gauge theories: the unified electroweak model and quantum chromodynamics [1].

The best theory of elementary particles we have at present is called, the Standard Model. This theory aims to explain all the phenomena of particle physics, except those due to gravity. It describes the strong, weak, and electromagnetic fundamental interactions, using mediating gauge bosons (the gluons, $W^{\pm}$ and Z bosons, and the photons), in terms of the properties and interactions of a small number of elementary particles. Finally, it predicted the existence of a type of boson known as the Higgs boson.

The currently accepted scientific theory is that our universe came into being some fifteen billion years ago in a gigantic explosion. Since then it has been continually growing and cooling down. The matter created in this explosion was subjected to unimaginable temperatures and pressures. As a result of these extreme conditions, reactions took place that were crucial in determining how the universe would turn out. The way that matter is structured now must reflect this common creation. Hence by building enormous and expensive accelerating machines and using them to smash particles together at very high energies, particle physicists can force the basic constituents of matter into situations that were common in the creation of the universe, they produce miniature big bangs. Hardly surprisingly, matter can behave in very strange ways under these circumstances [3].

The next section will describe in more detail the standard model and the most important current experiments in the study of particle physics the Large Hadron Collider (LHC) located at CERN in Geneva (Switzerland).

1.1 Standard Model

All in the visible Universe is found to be made from basic building blocks called fundamental particles, governed by fundamental forces. The best understanding of how these particles and forces are related to each other is encapsulated in the Standard Model (SM) of particles and forces. Developed in the early 1970s, it has successfully explained a host of experimental results and precisely predicted a wide variety of phenomena.

The fermions can be divided into two distinct groups called the quarks and the leptons (see Fig. 1.1), which are distinguished by the different ways in which they react to the fundamental forces. There are six different kinds of quarks and six leptons called flavors, which are related in pairs, or generations. The six flavors of quarks are called up(u), down(d), strange(s), charm(c), bottom(b) and top(t) (in order of mass). The six leptons are the electron(e), the electron-neutrino(ν_e), the muon(μ), muon-neutrino(ν_μ), tau(τ) and tau-neutrino(ν_τ).

All the quarks have important properties like charge, mass, color, lifetime, etc. One of the most important properties of quarks is that they interact via the strong force, which binds them into composite particles such as protons and neutrons. Quarks have not been observed

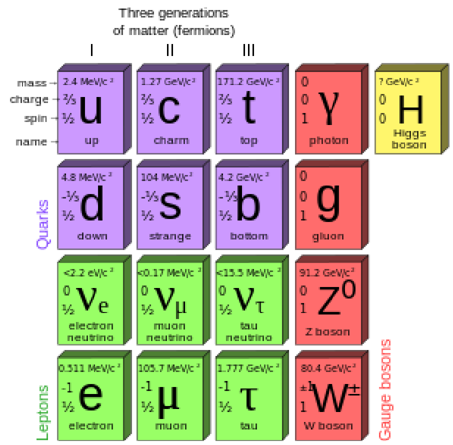

Figure 1–1: Elementary particles and gauge bosons.

in isolation, for this reason it is difficult to measure their mass. Leptons, in contrast, do not experience strong interactions and can be insolated as separate objects.

Gell-Mann and Zweig [4] proposed that quarks have an electric charge either 2/3 or -1/3, as compared to the -1 charge of the electron and the +1 charge of the proton. The Standard Model theory requires that each quark carries one of the three types of strong charge, also called color charge. There are two ways to make color-neutral combinations of quarks, called mesons (quark-antiquark combination) and baryons (combinations with three quarks), which together are referred to as hadrons [5]. The quark model predicts the combinations that exist with either spin $J = 1/2$ or spin $J = 3/2$.

After the above review about the particles, is important to know about interactions between all these particles. So far we know there are four fundamental forces: the strong force, the weak force, the electromagnetic force, and the gravitational force. They work over different ranges and have different strengths. Gravity is the weakest but it has an infinite range. The electromagnetic force also has infinite range but it is approximately thirty nine order of magnitude higher than gravity. The weak and strong forces are effective only over a very short range and dominate only at the level of subatomic particles.

The SM includes the electromagnetic, strong and weak forces all their carrier particles, and explains how these forces act on all the matter particles.

Each of these forces is mediated by the exchange of a particle (see photon, gluon, Z and W boson in Fig. 1.1):

• the *photon(γ)*, a quantum of light, carries no charges and is thus its own antiparticle, has zero mass, this is the carrier particle in electromagnetic interactions. Interactions between electrically charged particles can be viewed as being due to the exchange of photons between them.

• The carrier of the strong force field are called *gluons*, these particles like quarks, carry strong charges (color), and are confined and never seen as free particles. The strong interaction acts on all particles that have color charge, that is, on quarks and even on gluons themselves. The fact that strong force carrier particles themselves carry color is a fundamental difference between strong and electromagnetic interactions.

When a quark emits or absorbs a gluon, its color can change. The quarks within a hadron emit and absorb gluons frequently, and the hadrons remains color neutral, regardless of what exchanges occur inside it.

• There are two types of weak interaction carrier particles, the ones that carry electric charge are called W bosons (W^+ and its antiparticle W^-), and the one that is electrically neutral the Z^0 boson.

The weak interaction is the only interaction in which fundamental particles change flavor. $W^\pm$ bosons mediate all processes in which quark or lepton flavor is changed. The Z^0 boson in contrast cannot change flavor or electric charge.

• Standard Model does not include the theory of gravity and gravitons because no one yet knows how to make a satisfactory quantum theory of gravity. Like all other force fields, however, one expects there are carrier particles of the gravitational field, which are called *gravitons* [5].

Even with the great success of the Standard Models there is still much we would like to understand. Electromagnetism and the weak force are different manifestations of the same force, the electroweak force. Why then is the photon massless, whereas the $W^\pm$ and Z^0 bosons, have very large masses? The current best assumption, was associated with a postulated new field, called the Higgs field; its interaction does not cause a force on particles, rather it gives the particles their mass. Photons are massless because they do not interact with this field, while W and Z do interact and thereby get large masses. This theory led to the prediction of a new particle called the Higgs boson. For a long time a major goal of many experiments was to find the Higgs boson, which is an essential feature of the Standard Model.

With the recent observation at LHC of a new, Higgs-like particle with a mass of approximately 125 Gev the focus of searches for the standard model Higgs boson has shifted to evaluating the consistency of this new particle with SM expectations [6].

The discovery or exclusion of the SM Higgs boson is one of the primary scientific goals of the LHC. In 2012, an integrated luminosity of approximately 10 inverse femtobarns had been recorded by the experiments CMS and ATLAS and the proton-proton centre of mass energy was increased to 8 TeV, enhancing the sensitivity of the search for the Higgs boson. The result was the observation, by the two experiments, of a new heavy boson with a mass of approximately 125 GeV. The CMS publication focused on the observation in the five main decay channels in the lowmass range from 110 to 145 GeV: $H \to gg$, $H \to ZZ \to 4l$, $H \to WW \to lvlv$, $H \to \tau\tau$, and $H \to bb$, where l stands for leptons (electron or muon). The channels with the highest sensitivity for discovering the SM Higgs boson with a mass near 125 GeV are $H \to gg$ and $H \to ZZ \to 4l$. These channels are complementary for the way they are measured in the detector, and for the information they can provide about the SM Higgs boson [7].

In the SM present form, the quark and lepton masses or the mass of the Higgs boson can be predicted, these masses are simply parameters in the theory. One idea often pursued is that a theory would provide relationships among these parameters and would explain the odd set of values observed. Such theory would perhaps also tell whether any more quark or lepton types exist beyond the six of each is now known. Are there more force carrier particles? why does so much more matter than antimatter exist in the universe? are the quarks and leptons fundamental or are they composed of even more fundamental particles? what is the invisible, dark matter that seems to account for the majority of the mass of the universe? In this way there are many deeper questions that the Standard Model does not address.

Further, one of the goals of particle theory is to have a single universal theory that explains all the phenomena of the subject. Since we already have a unified theory for the weak and electromagnetic interactions, the next logical step is to try to include the strong interaction. Attempts to do this are called grand unified theories (GUTs) [8].

So far, how to write a satisfactory theory of gravity interacting with matter that includes all the well-known features of the Standard Model is not known. There is a class of theories known as string theories that show some promise for giving the desired combination of gravity and matter in a quantum framework, but nobody has found the way to incorporate all successful results of the Standard Model.

Besides, there is a indirect evidence that nature has a symmetry, called supersymmetry. Quantum theory tells that there are two kinds of particles, called fermions and bosons. For example, the matter particles (electrons and quarks) are fermions, while the particles whose exchange mediates the forces (photon, gluons, W and Z bosons) are bosons. The present description of particles and their interactions that shape the world treats the fermions and bosons very differently. Supersymmetry is the surprising idea that the fundamental theory actually treats fermions and bosons in a fully symmetric way. If they are interchanged, in the basic equations the resulting theory looks just like what you started with. One of its implications is that every particle has a superpartner, and that makes the theory very testable. If nature is indeed supersymmetric in a way that helps answer the above questions, the superpartners must exist, and some of them can be detected at LHC.

If supersymmetry indeed provides the explanation for some of what the Standard Model does not explain, it also implies a rather light Higgs boson exists, and that is another important test. Finding Higgs bosons at LHC is challenging for technical reasons but detecting the basic signals of the superpartners is likely to be easier since they produce a number of possible effects that can be distinguished from the Standard Model particles. Once the superpartners and the Higgs bosons are observed, their properties will help point the way to the form of the underlying theory and to how it answers the questions of the matter asymmetry and the dark matter and the identity of the inflation, and much more [9]. Now with the recent observation of the Higgs-like particle, many different studies are being carried out to find out if the supersymmetry is a consistent theory or not.

The LHC is a tool that provides, through its discoveries, what is needed to construct a more comprehensive theory that leads to the answers to these questions and many others [9].

1.2 The Large Hadron Collider

The LHC is the largest and most complex scientific undertaking ever attempted by the human beings. It is a particle accelerator used by physicists to study the smallest known particles, the fundamental building blocks of all things. It is revolutionizing the understanding, from the minuscule world deep within atoms to the vastness of the Universe. Its results determines the future of the full discipline of high energy physics. The LHC is built in a circular tunnel 26,659 km in circumference. The tunnel is buried around 50 to 175 m underground and straddles the Swiss and French borders on the outskirts of Geneva, Switzerland [10].

Two beams of subatomic particles called "hadrons" (protons) travel in opposite directions inside the circular accelerator (to avoid colliding with gas molecules inside the accelerator, the beams of particles travel in an ultra-high vacuum and internal pressure of 10^{-13} atm). Trillions of protons race around the LHC accelerator ring, travelling at 99.99 % the speed of light. Since protons are not elementary particles, collisions occur between two of their components (partons, i.e quarks and gluons), and this results in a high transferreed momentum in the direction transverse to the beam direction (p_T). These are called *hard collisions*, which usually contain the most interesting physics events. The effective centre-of-mass energy $\sqrt{s}$ is given by the centre-of-mass energy of the two partons [11].

The two beams of protons, in 2012 and 2011, each travelled at a maximum energy of 3.5 TeV, corresponding to head-to-head collisions of 7 TeV. The LHC 2012 run at a beam energy of 4 TeV, corresponding to a collision energy of 8 TeV, compared with the 7 TeV runs in 2010 and 2011. The data target for 2012 was 15 inverse femtobarns for ATLAS (and CMS), higher than the total until now. The LHC was scheduled to operate for two months in 2013 colliding protons with lead nuclei, and go into shutdown for upgrades to increase beam energy around 7 TeV per beam, with reopening planned for early 2015 [12]. After attaining the maximum energy of 14 TeV centre-of-mass energy at the end of 2014, it is expected that the LHC's will reach the design luminosity of 10^{34} $cm^{-2}s^{-1}$ in 2015. The magnets have two side-by-side apertures (dual-core or two-in-one design), one for each of the counter-rotating proton beams. The niobium-titanium coils create the magnetic fields to guide the two counter-rotating proton beams in separate magnetic channels, but within the same physical structure [13].

In LHC when two beams of protons collide, they generate temperatures more than 100,000 times hotter than the heart of the Sun, concentrated within a minuscule space. By contrast, the "cryogenic distribution system", which circulates superfluid helium around the accelerator ring, keeps the LHC at a super cool temperature of -271.3^0C (1.9 K).

The protons of the LHC circulate around the ring in well-defined bunches. The bunch structure of a modern accelerator is a direct consequence of the radio frequency (RF) acceleration scheme. In the LHC, under nominal operating conditions, each proton beam has 2,808 bunches, with each bunch containing about 10^{11} protons. Increasing the number of bunches is one of the ways to increase luminosity in a machine.

The particles are so tiny that the chance of any two colliding is very small. When the bunches cross, there are a maximum of about 20 collisions between 200 billion particles. Bunches cross on average about 30 million times per second, so the LHC generates up to 600 million particle collisions per second. Only a small fraction that have interesting characteristis is recorded. For example, one in every 10,000 particles emerging from the collisions is a high energy electron or muon [14].

The power and energy figures for the LHC are very impressive. If the total energy of each LHC beam is calculated, then is obtained:
$2808*1.15*10^{11}$ protons per bunch $*7\ TeV = 0.185\ M_{Planck} = 362\ MJ$. The accurate steering of the beam at all times is essential.
The *instantaneous luminosity* at the LHC is:

$$L = \frac{n_b N_L N_R f_{rev}}{A_T^{eff}} \sim 10^{34}\ cm^{-2}s^{-1},$$

where the revolution frequency $f_{rev} = c/27\ km \sim 10^4 Hz$, n_b is the number of bunches per beam, N_L and N_R are the numbers of particles in the bunches of each colliding beam, and $A_T^{eff} = 4\pi\sigma_b^2$ is the effective transverse area (cross section) of the proton beam and with $\sigma_b = 16\ microns$. The total inelastic (non-diffractive) cross section is about 60 millibarns a $(1barn = 10^{-24}\ cm^2)$. The collision rate, is $L * \sigma \sim 10^9\ Hz$: a billion per second.

The *integrated luminosity* is: $\int_{year} Ldt = 100\ fb^{-1}$.

One year is about $\pi * 10^7\ s$. Empirically a collider operates about $1/\pi$ of the time a year and it is customary to take 1 "collider year" to be $10^7\ s$. The integrated luminosity over a year at the LHC at design luminosity is then $10^{41}cm^{-2}$ or 100 fb^{-1}.

Physicists use the LHC to recreate the conditions just after the Big Bang, by colliding the two beams head-on at very high energy. Teams of physicists from around the world analyse the particles created in the collisions using special detectors in a number of experiments dedicated to the LHC.

The purpose of a detector is to record as accurately and completely as possible the properties of the particles that are produced in collisions. We often need to study millions of events in order to unravel the physical processes that occur in particle physics experiments. A detector must therefore, be able to record the events at a high rate. High speed computers are needed to analyze these data at a rate comparable with the recording rate. The detector reconstructs each event as fully as possible by measuring the momentum, energy, and trajectory of the final state particles. From these observations, we can determine the particle type [5].

The data recorded by each of the big experiments at the LHC fills around 100,000 dual layer DVDs every year. To allow the thousands of scientists scattered around the globe to collaborate on the analysis over the next 15 years (the estimated lifetime of the LHC), tens of thousands of computers located around the world are being harnessed in a distributed computing network called the Grid.

There are six experiments installed at the LHC: A Large Ion Collider Experiment (ALICE), A Toroidal LHC ApparatuS (ATLAS), the Compact Muon Solenoid (CMS), the Large Hadron Collider beauty (LHCb) experiment, the Large Hadron Collider forward (LHCf) experiment and the TOTal Elastic and diffractive cross section Measurement (TOTEM) experiment. They are installed in four huge underground caverns built around the four collision points of the LHC beams (see Fig. 1.2).

ALICE (aiming at a peak luminosity of $10^{27}cm^{-2}s^{-1}$ for nominal lead-lead ion operation) is a detector specialized in analysing lead-ion collisions. It studys the properties of quark-gluon plasma, a state of matter where quarks and gluons, under conditions of very high temperatures

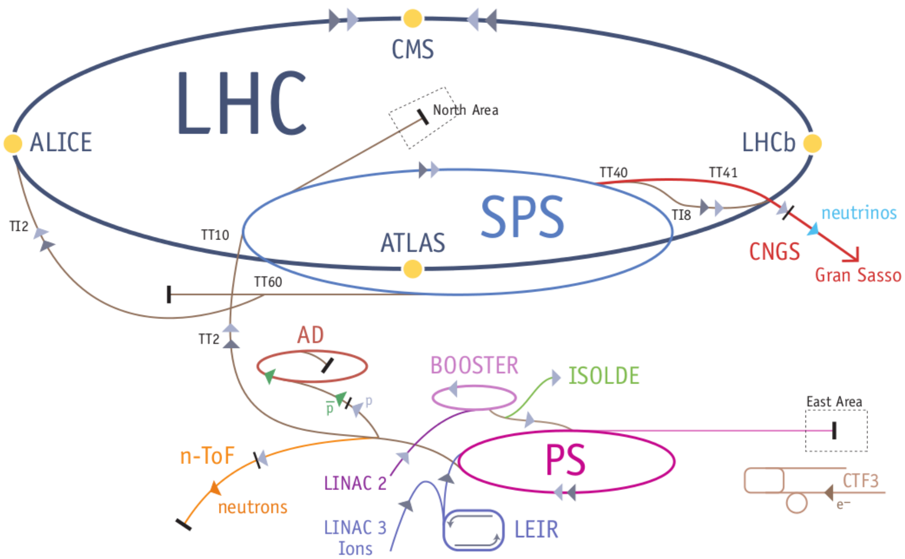

Figure 1–2: LHC - Large Hadron Collider and its experiments, CMS, ATLAS, ALICE, LHCb, TOTEM

and densities, are no longer confined inside hadrons. Such a state of matter probably existed just after the Big Bang, before particles such as protons and neutrons were formed.

ATLAS and CMS (aiming at a peak luminosity of $10^{34} cm^{-2} s^{-1}$ for proton operation) are general purpose detector designed to cover the widest possible range of physics at the LHC, from the search for the Higgs boson to supersymmetry (SUSY) and extra dimensions. ATLAS is the largest-volume collider-detector ever constructed. CMS is built around a superconducting solenoid. This takes the form of a cylindrical coil of superconducting cable that generates a magnetic field of 4T.

LHCb aiming at a peak luminosity of $10^{32} cm^{-2} s^{-1}$, is a specialized b-physics experiment, that is measuring the parameters of CP violation in the interactions of b-hadrons (heavy particles containing a bottom quark). Such studies can help to explain the Matter-Antimatter asymmetry of the Universe. The detector is also able to perform measurements of production cross sections and electroweak physics in the forward region.

LHCf is a small experiment that measures particles produced very close to the direction of the beams in the proton-proton collisions at the LHC. The motivation is to test models used to estimate the primary energy of the ultra high-energy cosmic rays.

TOTEM (aiming at a peak luminosity of $2 \times 10^{29} cm^{-2} s^{-1}$ with 156 bunches) measures the effective size or cross-section of the proton at LHC. To do this TOTEM must be able to detect particles produced very close to the LHC beams.

In the University of Puerto Rico Mayaguez, the High Energy Physics group is currently working in the experiment Compact Muon Solenoid CMS at the Large Hadron Collider LHC at CERN. Hence, at this point, is important to do a better description of this experiment from where is obtained the data, which is the base of this work. In the next chapter the CMS experiment is explained in more detail.

Chapter 2
CMS EXPERIMENT

The Compact Muon Solenoid (CMS) experiment uses a general-purpose detector to investigate important issues in particle physics, including the search for the Higgs boson (with respect to this, in 2012 July 4 was announced a Higgs-like boson in this experiment and ATLAS), extra dimensions, and particles that could make up dark matter. CMS is designed to identify most of the very energetic particles emerging from the proton-proton collisions, and to measure as efficiently and precisely as feasible their trajectories and momentum [13].

The overall layout of CMS is shown in Fig. 2–1. At the heart of CMS sits a 13-m-long, 5.9 m inner diameter, 4 T superconducting solenoid; the overall dimensions of the CMS detector are a length of 21.6 m, a diameter of 14.6 m and a total weight of 12,500 tons. In order to achieve good momentum resolution within a compact spectrometer without making stringent demands on muon-chamber resolution and alignment, a high magnetic field was chosen [15].

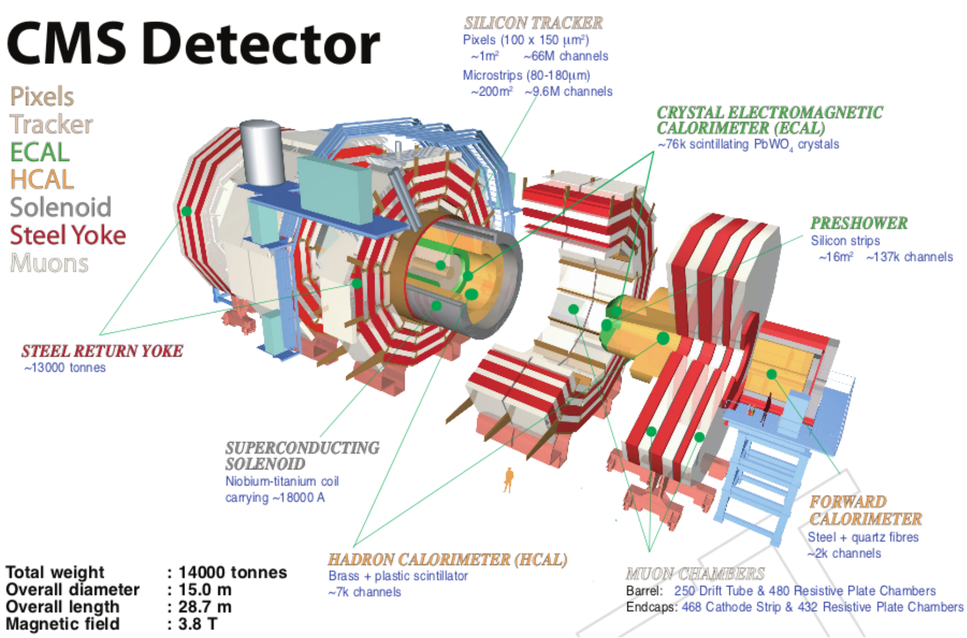

Figure 2–1: CMS Detector parts. Size: 21 m long, 15 m wide and 15 m high, Weight: 12,500 t, Design: barrel plus end caps, Location: Cessy, France.

The coordinate system adopted by CMS has the origin centered at the nominal collision point inside the experiment, the y-axis pointing vertically upward, and the x-axis pointing radially inward toward the center of the LHC. Thus, the z-axis points along the beam direction. The azimuthal angle φ is measured from the x-axis in the $x - y$ plane. The polar angle θ is measured from the z-axis (Fig. 2–2).

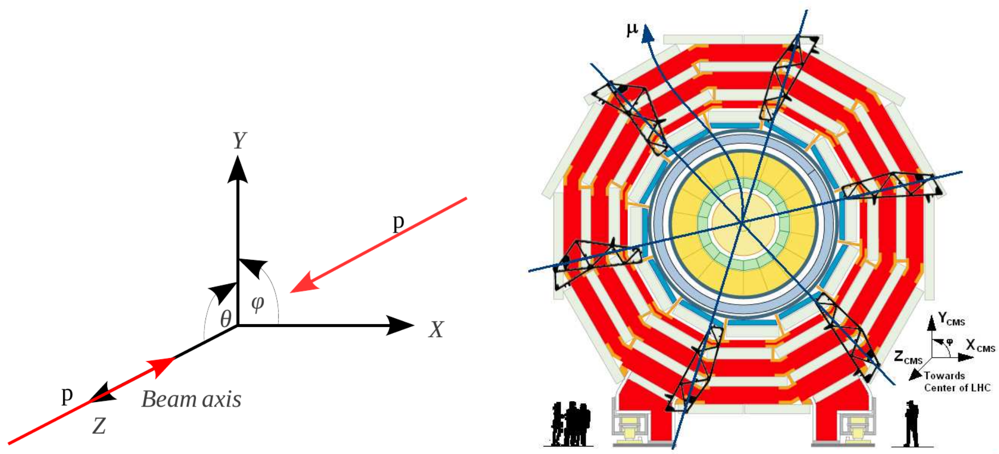

Figure 2–2: CMS transversal view and $x,\ y,\ z$ coordinates.

In a pp collision, with z -axis pointing along the beam direction, rapidity is a variable used to describe the behaviour of particles in inclusively measured reactions

$$y = \tfrac{1}{2}\ln\left(\tfrac{E+p_{\mathrm{L}}}{E-p_{\mathrm{L}}}\right)$$

where p_L is the longitudinal momentum along the direction of the incident particle, E is the energy, both defined for a given particle.

In the limit where the particle is travelling close to the speed of light the rapidity (y) becomes to the pseudorapidity η, which is

$$\eta = \text{-log}[\tan(\theta/2)]$$

Using these parameters, the distance between two particles can be defined as

$$\Delta R = \sqrt{\Delta\varphi^2 + \Delta\eta^2}$$

Thus, the momentum and energy measured transverse to the beam direction, denoted by p_T and E_T, respectively, are computed from the x and y components. The imbalance of energy measured in the transverse plane is denoted by E_T^{miss} [16].

The interesting particles are produced over a wide range of energies (from a few hundred MeV to a few TeV) and over the full solid angle. They therefore need to be detected down to small polar angles (θ) with respect to the incoming beams [13].

The interaction point, is the point around the center of the detector at which proton-proton collisions occur between the two counter-rotating beams of the LHC. At each end of the detector magnets focus the beams into the interaction point. At collision each beam has a radius of 17 μm and the crossing angle between the beams is 285 μrad.

Moving outward from the interaction region, the experiment have a tracking system to measure the directions and momenta of all possible charged particles emerging from the interaction vertex; an electromagnetic and a hadronic calorimeter system to absorb and measure the energies of electrons, photons, and hadrons, and outer layers of muon detectors dedicated to the measurement of the directions and momenta of high-energy muons [13].

2.1 CMS Components

2.1.1 CMS Tracker

Momentum of particles is crucial in helping us build up a picture of events at the heart of the collision. One method to calculate the momentum of a particle is to track its path through a magnetic field; the more curved the path, the less momentum the particle had (where the momentum in this case is $P = qRB$, being R the radius of curvature in the plane perpendicular to the magnetic field (B), and q the electric charge of the particle). The CMS tracker contained in the central solenoid provides efficient tracking of charged particles within the pseudorapidity range $|\eta| < 2.5$, allowing the momentum measurement of charged particles and the reconstruction of primary and secondary vertices [13].

The tracker can reconstruct the paths of high-energy muons, electrons and hadrons as well as see tracks coming from the decay of long-lived particles such as beauty or b quarks that will be used to study the differences between matter and antimatter.

Because of the tracking detector is so close to the collision, the number of particles passing through is very large: the rate of particles received 8 cm from the beam line will be around 10 million particles per square centimeter per second. The pixel detector is able to disentangle and reconstruct all the tracks they leave behind (see Fig. 2–3).

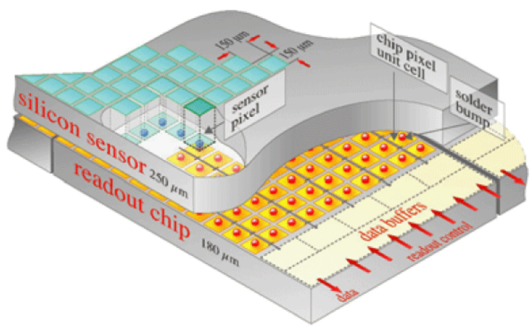

Figure 2–3: Pixel detector, each layer is split into segments like tiny kitchen tiles, each a little silicon sensor, 100 μm by 150 μm.

When a charged particle passes through the pixel detector, it gives enough energy for electrons to be ejected from the silicon atoms, creating electron-hole pairs. Each pixel uses an electric current to collect these charges on the surface as a small electric signal that are amplified and detected. The tracker employs sensors covering a total area to the size of a tennis court, with 75 million separate electronic read-out channels: in the pixel detector there are some 6,000 connections per square centimeter.

After the pixels and on their way out of the tracker, particles pass through ten layers of silicon strip detectors, which consists of four inner barrel (TIB) layers assembled in shells with two inner endcaps (TID), each composed of three small discs. The outer barrel (TOB) consists of six concentric layers. Finally two endcaps (TEC) close off the tracker (see Fig. 2–4).

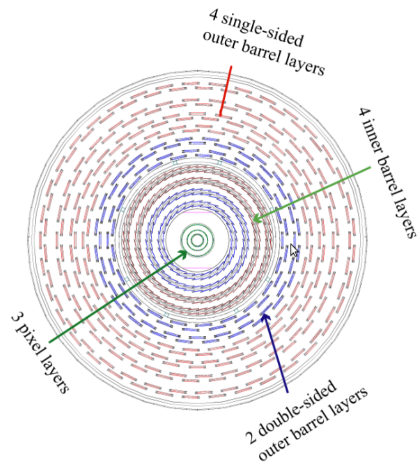

Figure 2–4: Silicon strip detectors, inner barrel (TIB), inner endcaps (TID), outer barrel (TOB).

2.1.2 Electromagnetic Calorimeter (ECAL)

In order to build up a picture of events occurring in the LHC, CMS must find the energies of emerging particles. Of particular interest are electrons and photons, because of their use in finding the Higgs boson and other new physics.

The ECAL (cylindrical barrel consists of 61,200 crystals formed into 36 supermodules) provides coverage up to $|\eta| = 3$ and uses lead tungstate ($PbWO_4$) crystals. With a touch of oxygen in this crystalline form it is highly transparent and scintillates when electrons and photons pass through it. The light (it produces light in proportion to the particle's energy) is detected by silicon avalanche photo-diodes (APDs) in the barrel and vacuum phototriodes (VPTs) in the endcaps. A preshower system is installed in front of the endcap ECAL for π^0 rejection [17].

In CMS, when a high-energy electron or photon collides with the heavy nuclei of the ECAL crystals, it generates a shower of electrons, positrons and photons, and atoms in the material take energy from the passing particles to excite their electrons. The atoms quickly relax and the electrons each emit the extra energy as a photon of blue light. A photo device then picks up these scintillation photons and the amount of light generated is proportional to the energy that was deposited in this crystal. This tells us the energy of the incoming electron or photon.

2.1.3 Hadron Calorimeter (HCAL)

The Hadron Calorimeter (HCAL) (Covers pseudorapidities between 3.0 and 5.0) measures the energy of hadrons, particles made of quarks and gluons (for example protons, neutrons, pions and kaons). Additionally it provides indirect measurement of the presence of non-interacting, uncharged particles such as neutrinos.

The design of HCAL is strongly influenced by the choice of magnet parameters since most of the CMS calorimetry is located inside the magnet coil and surrounds the ECAL system. An important requirement of HCAL is to minimize the non-Gaussian tails in the energy resolution and to provide good containment and hermeticity for the E_T^{miss} measurement [16].

The HCAL is a sampling calorimeter, meaning it finds a particle's position, energy and arrival time using alternating layers of absorber and fluorescent scintillator materials that produce a rapid light pulse when the particle passes through. Special optic fibres collect this light and feed it into readout boxes where photodetectors amplify the signal.

2.1.4 CMS Magnet

The CMS magnet is a solenoid, a magnet made of coils of wire that produce a uniform magnetic field when electricity flows through them. The CMS magnet is "superconducting", allowing electricity to flow without resistance and creating a powerful magnetic field. This magnet was designed to reach a 4 T field in a free bore of 6 m diameter and 12.5 m length with a stored energy of 2.6 GJ at full current. The distinctive feature of the 220 ton cold mass is the four layer winding made from a stabilized reinforced NbTi conductor. The ratio between stored energy and cold mass is critically high (11.6 KJ/kg), causing a large mechanical deformation (0.15 %) during energizing, well beyond the values of any solenoidal detector magnets built to-date [13].

Its job is to bend the paths of particles emerging from high-energy collisions in the LHC. The more momentum a particle has the less its path is curved by the magnetic field, so tracing its path gives a measure of momentum. CMS began with the aim of having the strongest magnet possible because a higher strength field bends paths more and, combined with high-precision position measurements in the tracker and muon detectors, this allows accurate measurement of the momentum of even high-energy particles.

The tracker and calorimeter detectors (ECAL, HCAL) fit snugly inside the magnet coil whilst the muon detectors are interleaved with a 12-sided iron structure that surrounds the magnet coils and contains and guides the field. The enormous magnet also provides most of the experiment's structural support, and must be very strong itself to withstand the forces of its own magnetic field.

2.1.5 Muon system

As the name Compact Muon Solenoid suggests, detecting muons is one of CMS's most important tasks, providing independent muon tracking to improve muon reconstruction, especially at high momenta. In this context the muon system has 3 special functions: muon identification, momentum measurement and triggering over the entire kinematic range of the LHC. Centrally produced muons are measured 3 times: in the inner tracker, after the coil, and in the return flux. Measurement of the momentum of muons (which are 200 times heavier than electrons and positrons) using only the muon system is essentially determined by the muon bending angle at the exit of the 4 T coil (which lead to an excellent muon momentum resolution and trigger capability, and serves as a hadron absorver to facilitate the identification of muons), taking the interaction point as the origin of the muon.

The resolution of this measurement is dominated by multiple scattering in the material before the first muon station up to p_T values of 200 GeV/c, when the chamber spatial resolution starts to dominate. For low-momentum muons, the best momentum resolution is given by the resolution obtained in the silicon tracker [16].

Because muons can penetrate several meters of iron without interacting, unlike most particles they are not stopped by any of CMS's calorimeters. Therefore, chambers to detect muons are placed at the very edge of the experiment where they are the only particles likely to register a signal.

A particle is measured by fitting a curve to hits among the four muon stations (see Fig. 2–5), which sit outside the magnet coil and are interleaved with iron return yoke plates (shown in red, for the barrel region). By tracking its position through the multiple layers of each station, combined with tracker measurements the detectors precisely trace a particle's path.

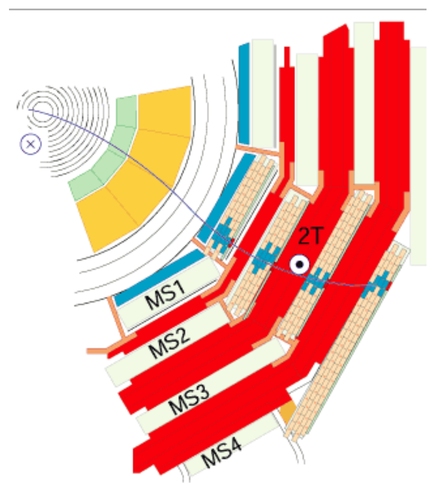

Figure 2–5: Four muon stations, sit outside the magnet coil and are interleaved with iron return yoke plates.

Three types of gaseous detectors are used to identify and measure muons. The choice of the detector technologies has been driven by the very large surface to be covered and by the different radiation environments. In the barrel region ($|\eta| < 1.2$), where the neutron induced background is small, the muon rate is low and the residual magnetic field in the chambers is low, drift tube (DT) chambers are used (The Barrel Detector, consisting of 250 chambers organized in 4 layers, stations labeled MB1, MB2, MB3 and MB4 (see Fig. 2–6) with the last being the outermost).

In the two endcaps, where the muon rate as well as the neutron induced background rate is high, and the magnetic field is also high, cathode strip chambers (CSC) (The Muon Endcap (ME) system comprises 468 CSCs in the 2 endcaps) are deployed and cover the region up to $|\eta| < 2.4$. In addition to this, resistive plate chambers (RPC) are used in both the barrel and the endcap regions, in the first endcap station are used to help resolve ambiguities in the CSCs. There are 36 chambers mounted in each of 2 rings in each of the endcap stations [16].

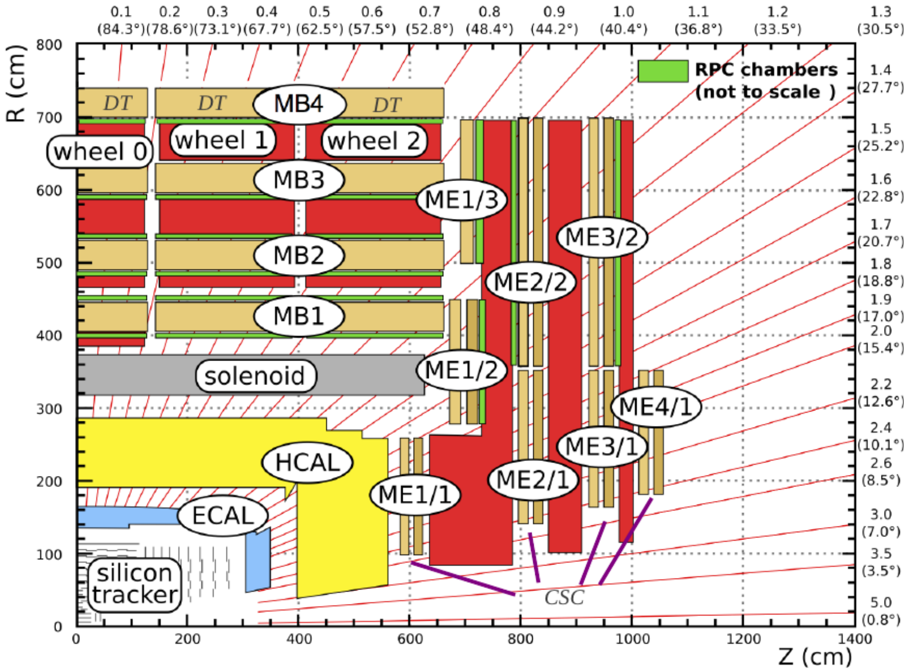

Figure 2–6: Layout of one quarter of the CMS muon system for initial low luminosity running. The RPC system is limited to $|\eta| < 1.6$ in the endcap, and for the CSC system only the inner ring of the ME4 chambers have been deployed.

In order to understand how the CMS experiment design is a key to perform the event selection and reconstruction, a brief explanation is given in this paragraph. As is described in chapter 2, the central feature of the CMS experiment is that it has a superconducting solenoid. Within the field volume are the silicon tracker, the electromagnetic calorimeter, and the hadron calorimeter. Muons are detected in the interval $|\eta| < 2.2$ by gaseous detectors made of three technologies: DT, CSC and RPC, embedded in the steel return yoke; the measured points in these detectors determine the bending curvature, which in turn provides a measurement of the inverse momentum (using the Lorentz force) and the charge of a muon (analizing the bend direction).

Some CMS detector general requirements to meet the LHC's goals can be summarized as follows:

• Good muon identification and momentum resolution in the region $|\eta| < 2.2$, the transverse momentum of muons matched to reconstructed tracks is measured with a resolution better than 1.5% for p_T smaller than 100 GeV/c, good dimuon mass resolution.

• Good charged particle momentum resolution and reconstruction efficiency in the inner tracker.

• Good electromagnetic energy resolution, good diphoton and dielectron mass resolution, wide geometric coverage, correct localization of the primary interaction vertex.

• Good E_T^{miss} and dijet mass resolution

Thanks to a high magnetic field, a full inner tracking system and a fully scintillating electromagnetic calorimeter, the CMS experiment meets the requirements. However, there are many factors restricting the capability of the muon system to measure accurately, for example: the momentum of a muon, multiple scattering in the calorimeters and in the thick steel plates separating the muon stations, energy loss, detectors resolution, chamber misalignment and uncertainty of B field, etc [18]. To address these factors an analysis of systematic uncertainties is done, which will be shown later.

In the next sections the data selection is described. It covers the datasets used, event selection and reconstruction, which is related with each particle of interest, and the corresponding selection cuts.

2.1.6 CMS Event Selection and Reconstruction

The job of a particle detector is to record and visualise the explosions of particles that result from the collisions at accelerators. The information obtained on a particle's speed, mass, and electric charge help physicists to work out the identity of the particle.

The overall collection of software, referred to as CMSSW, is built around a Framework [1], an Event Data Model (EDM), and Services needed by the simulation, calibration and alignment, and reconstruction modules that process event [2] data so that physicists can perform analysis. The primary goal of the Framework and EDM is to facilitate the development and deployment of reconstruction and analysis software [20].

---

[1] A software framework is an abstraction in which software providing generic functionality can be selectively changed by additional user written code, thus providing application specific software. A software framework is a universal, reusable software platform used to develop applications, products and solutions [19].

[2] Physically, an event is the result of a single readout of the detector electronics and the signals that will have been generated by particles, tracks, energy deposits, present in a number of bunch crossings.

The CMS Event Data Model (EDM) is centered around the concept of an Event. An Event is a C++ object container for all RAW (Detector data after online formatting, the L1 trigger result, the result of the High-Level Trigger selections, which are going to be explained in the next subsection) [21] and reconstructed data related to a particular collision. During processing, data are passed from one module to the next via the Event, and are accessed only through the Event. All objects in the Event may be individually or collectively stored in ROOT files, and are thus directly browsable in ROOT (is an analysis package written in an object-oriented structure in C++. It uses built-in functions and user-compiled code to produce graphics and histograms, as well as trees with data objects) [22].

The reconstruction process is seen as a collection of independent units, each one providing a set of corresponding reconstructed objects as output. The reconstruction process can be divided into three steps, corresponding to local reconstruction within an individual detector module, global reconstruction within a whole detector, and combination of these reconstructed objects to produce higher-level objects.

The reconstruction units providing local reconstruction in a detector module use as input real data from the DAQ (Data Acquisition) system [3] or simulated data representing the real data. The output from the reconstruction units are reconstructed hits (RecHits) which contain information about the energy deposition and positions of the particles interacting in the detectors (from times or clusters of strips or pixels).

In the Muon Drift Chambers (DTs), local reconstruction provides the position of a muon hit in a drift cell, determined from the drift time measurement and the effective drift velocity.

In the Muon Cathode Strip Chambers (CSCs), local reconstruction provides position and time of arrival of a muon hit from the distribution of charge induced on the cathode strips. In the Muon Resistive Plate Chambers (RPCs), local reconstruction gives the position of a muon hit from the position of clusters of hit strips.

[3] The task of the online Trigger and Data Acquisition System is to select, out of the millions of events recorded in the detector, the most interesting 100 or so per second, and then store them for further analysis.

In the Electromagnetic Calorimeter (ECAL), local reconstruction identifies the position, time of arrival, and energy of localized electromagnetic energy depositions.

In the Hadron Calorimeter (HCAL), local reconstruction likewise identifies the position, time, and energy of localized hadronic energy depositions.

The RecHits are added to the event, and used as the input to the global reconstruction. In the global reconstruction step information from the different modules of a subdetector are combined. For example, Tracker RecHits (reconstructed hits from the Tracker system) are used to produce reconstructed charged particle tracks and Muon RecHits (reconstructed hits from the Muon system) are used to produce candidate muon tracks.

The final reconstruction step combines reconstructed objects from individual subdetectors to produce higher-level reconstructed objects suitable for high-level triggering or for physics analysis. For example, tracks in the Tracker system and tracks in the Muon system are combined to provide final muon candidates, and electron candidates from the Calorimeter system are matched to tracks in the Tracker system [16].

Chapter 3
Λ_b^0 GENERAL PROPERTIES

After giving a general description about the CMS experiment in which we rely to make this work, it is important to give a brief introduction about the decay subject of this study, starting with the description of the Λ_b^0 decay.

Λ_b^0 is a particle known as a baryon which are particles made of three quarks in bound state. The quark model predicts that the baryon combinations exist as objects with either spin J=1/2 or spin J=3/2. The Fig. 3 shows the various three-quark combinations with J=1/2 that are possible using the three lightest quarks (up, down and strange) and the bottom quark [23].

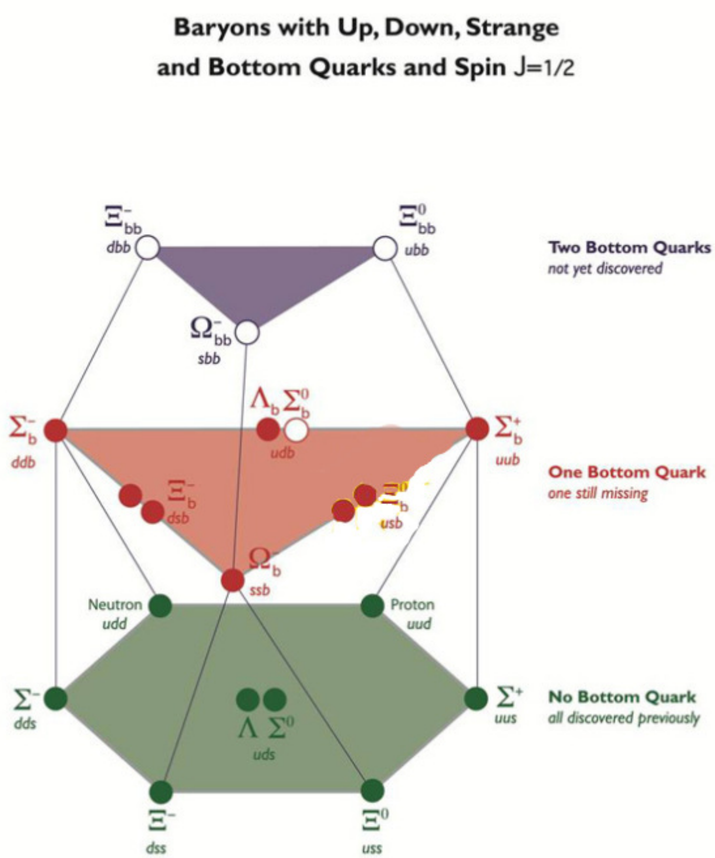

Figure 3–1: Three-quark combinations (baryobs) with $J = 1/2$ that are possible using the three lightest quarks (up, down and strange) and the bottom quark.

The Mendelev of elementary particle physics was Murray Gell-Mann, who introduced the so-called Eightfold Way 1961, that arranged the baryons and mesons into weird geometrical patterns, according to their charge and strageness [24]. The eight lightest baryons fit into hexagonal array, the botton part of the Fig. 3. In this diagram the proton and neutron contain no strange quarks. The proton contains two u quarks and one d quark, while the neutron contains one u quark and two d quarks. The electric charge of the proton is 1 (2/3 + 2/3 - 1/3 = 1), while the neutron has charge 0 (2/3 - 1/3 - 1/3 = 0). The baryons in the middle row (of the octet in the bottom part of the Fig. 3) all have strangeness -1, and the others (Ξ^-, Ξ^0) have strangeness -2. The Σ^- is dds, the Σ^+ is uus, and the Λ^0 and Σ^0 are both uds.

Experiments at Fermilab's Tevatron collider have discovered all of the observed baryons with one bottom quark except the Λ_b^0 which was definatly discovered at CERN. There exist additional baryons involving the charm quark, which are not shown in this graphic.

The Lambda baryons are a family of subatomic hadron particles which have +1 elementary charge or are neutral. They are baryons containing three different quarks: one up, one down, and one third quark, which can be either a strange, a charm, a bottom or a top quark. The first Lambda particle discovered was Λ^0 in 1947 during a study of cosmic ray interactions. The first evidence for Λ_b^0 (the lightest b baryon composed of quarks u, d and b) existence was reported by CERN and Fermilab in late 1990s based on a handful of events, this is an electrically neutral baryon having a mass 11,000 times that of the electron, a mean lifetime of approximately 1.1×10^{-12} seconds and a rest mass of $5,620.2 \pm 1.6$ MeV$/c^2$ [25].

Because of its relative abundance, the Λ_b^0 baryon has been used to investigate production and decay properties of heavier b baryons, to search for possible polarization effects, for violation of discrete symmetries in the decay (CP and T violation), and to search for Beyond Standar Model (BSM) effects.

For the Λ_b^0 baryon, only a few decay channels have been studied, and the uncertainties on its branching fractions are large, $\sim$ 30-60%. For higher mass b baryon states (B_c, Ω_b, Ξ_b and Σ_b), even less information is available. For these reasons the physics of Λ_b^0 provide a unique window on B physics [26].

One of the decay channels of Λ_b^0 is $\Lambda_b^0 \to \Lambda^0 J/\psi$ and was the first successful measurement of the exclusive hadronic decay rate of bottom baryons, it was done at CERN $p\overline{p}$ collider, using 4.7 pb^{-1} of muon data collected in the 1988/89 [27]. In analogy to s bottom meson (B) hadronic decays, where the B has been observed in both $B \to J/\psi X$ and $B \to \psi(2S)X$ mode, in the Λ_b^0 only the J/ψ mode has been observed until now.

This thesis is focused on the search for the $\Lambda_b^0 \to \Lambda^0\psi(2S)$ decay and on the reconstruction of the $\Lambda_b^0 \to \Lambda^0 J/\psi$ decay (normalizing mode) as our learning tool. This latest mode has higher statistics and lead a direct tuning of the analysis algorithms on data.

In both of the decays the original b-quark from the Λ_b^0 is transformed by a W boson into a s-quark, which bound with the quark u and d from the Λ_b^0 to form the Λ^0 (uds) baryon (Fig. 3–2).

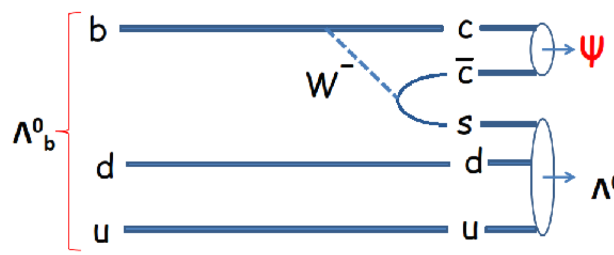

Figure 3–2: Cabibbo favoured Λ^0 plus a charmonium state (ψ).

Transitions between quarks of different flavors occur only due to the weak interaction, like in the decay $\Lambda_b^0 \to \Lambda^0\psi(2S)$ or Λ^0 , as is shown in Fig. 3–2, where the J/ψ and $\psi(2S)$ are mesons composed of a charm (c) and anti-charm ($\bar{c}$) quarks in bound state. Only quarks with the same charge can mix. Due to the explicit form of the weak interaction, it is only necessary to consider mixing of the $-1/3$ quarks (this induces transitions involving the $+2/3$ quarks also). The mixing is treated mathematically via the unitary Cabibbo-Kobayashi-Maskawa (CKM) matrix. This decay presents two flavor changes, $b \to s$ and the transformation of a W^- in s and $\bar{c}$. The first transition is called Cabibbo-Supressed because is between quarks from different families. The second one is called Cabibbo-Favoured, this transformations within families are much more likely [28], [29].

Nowadays, studies of this type of baryons are carried out at Fermilab and CERN Large Hadron Collider, but their experimental knowledge is still limited. However, many experimental updates are achieved, leading to obtain higher luminosity,s higher energy at the LHC and with the large heavy flavor production cross-section at these energies, b baryons becomes more experimentally accessible to measure with improved precision important measurements, such as lifetime, polarization, CP and T violation, and even new b baryons [30] and new decay modes such as the one presented in this work.

To take advantage of the large b quark cross-section at LHC, the CMS has implemented a novel trigger strategy based on the long lifetime of b hadrons to reconstruct vertices and tracks displaced from the primary interaction, which allows identification of long lived particles as Λ_b^0.

The LHC provides pp collisions at high interaction rates (25 ns beam crossing interval $\rightarrow$ 40 MHz crossing frequency) leads to 10^9 interactions/sec. It is impossible to store and process the data associated to the high number of events, hence the trigger system has to perform a drastic rate reduction with the called Level-1 (L1) trigger (a hardware-based trigger) that involves the calorimeters and muon systems and the High-Level Trigger (HLT) (software-based trigger, access the read-out data and perform complex calculations), which reduce the L1 output rate by 99.99% (from 100,000 Hz to 100 Hz) for mass storage and offline further studies.

Further requirements at the HLT level have been applied in this work: the measurements given here are based on dimuon events belong to the final Λ_b^0, from which the signal and the normalization mode are triggered by the dimuon High-Level Trigger (HLT) called the displaced low dimuon mass trigger (LMT).

In addition, the experiment's silicon tracker (pixels and strips) gives excellent transverse momentum (p_t) and vertex resolutions that combined with the muon system yields a high resolution dimuon invariant mass sample, which is used, in combination with $\Lambda^0 \rightarrow p\pi^-$ to reconstruct a $\Lambda_b^0 \rightarrow \Lambda^0\mu^+\mu^-$ candidate sample as our initial sample.

In the process of purifying the $\Lambda_b^0 \rightarrow \Lambda^0\mu^+\mu^-$ sample from the most copious "*charmed*" Cabibbo Favoured $\Lambda_b^0 \rightarrow \Lambda^0 J/\psi$ decay, the $\Lambda_b^0 \rightarrow \Lambda^0\psi(2S)$ decay mode is observed for the first time, being the main purpose of this work. They are topologically equivalent to $\Lambda_b^0 \rightarrow \Lambda^0\mu^+\mu^-$, Λ^0 $\psi(2S)$ and Λ^0 J/ψ, where $\psi(2s)$ decays in $\mu^+\mu^-$ as well as J/ψ and Λ^0 decays into a $p(uud)\pi^-(d\bar{u})$.

Analysis of the particles concerning this decay is done taking advantage of excellent performances of the muon detection system and silicon tracker which, combined, yields to precise measurements of charge particle trajectories, transverse momentum, vertices and a high resolution dimuon invariant mass.

Chapter 4
OBJECTIVES

The general objective of this thesis is to report the first observation of the exclusive baryonic $\Lambda_b^0 \rightarrow \Lambda^0\psi(2S)$ (with $\psi(2S) \rightarrow \mu^+\mu^-$ and $\Lambda^0 \rightarrow p\pi^-$) decay, working with data sample recorded on 2011 by the CMS experiment at the LHC in pp collisions at $\sqrt{s} = 7\ TeV$ with an integrated luminosity of 5.3 fb^{-1}. At present, this Λ_b^0 decay is not reported by the Particle Data Group (PDG) and is not yet as official approved result in the CMS collaboration.

This study will measure the $\Lambda_b^0 \rightarrow \Lambda^0\psi(2S)$ Branching Ratio relative to the $\Lambda_b^0 \rightarrow \Lambda^0 J/\psi$ (with $J/\psi \rightarrow \mu^+\mu^-$) production, in other words the B($\Lambda_b^0 \rightarrow \Lambda^0\psi(2S)$) is normalized with respect to the most copious Cabibbo favoured $\Lambda_b^0 \rightarrow \Lambda^0 J/\psi$ decay channel.

The possible sources of systematic uncertainties are analyzed mainly in the determination of the Λ_b^0 yields, the determination of the relative efficiency, the different contaminations ($B^0 \rightarrow J/\psi K^0_{short}$ or $B^0 \rightarrow \psi(2s)K^0_{short}$ decays), etc. All these systematic uncertainties are combined assuming no correlations between them.

This work is based on the CMS experiment Muonia dataset, which is an enriched sample of dimuons, and most of this kind of analysis starts with the dimuon pair reconstruction. In this case the analysis started by reconstructing first the $\Lambda^0 \rightarrow p\pi^-$ decay and then the muon pair coming from the J/ψ or $\psi(2S)$ meson to look the dimuons associated to the Λ^0.

The selection criteria is a group of parameters such as transverse momentum, vertices distance, impact parameter significance, pseudorapidity region, "pointing angle", invariant mass constraints, etc, which in this analysis are used to identify the particles used in Λ_b^0 hadron reconstruction. Precise measurements of charge particle trajectories and reconstruction of secondary vertices are crucial for this analysis.

Muons from signal ($\psi(2S)$) and normalization (J/ψ) mode in the final Λ_b^0 have to match the High Level Trigger (HLT) called displace low mass trigger (LMT) in order to ensure the dimuon candidates were tagged by the trigger.

In addition, the Monte Carlo (MC) samples are treated in the same way as data and are used to check the agreement with data, to tune the selection criteria and to find out the reconstruction efficiency for these processes.

Chapter 5
ANALYSIS AND RESULTS

5.1 Data Sample

In this analysis the data sample consist of an integrated luminosity of 5.3 fb^{-1}, recorded by the CMS experiment at the LHC during 2011 with pp collisions at the centre-of-mass energy of $\sqrt{\mathbf{s}} = 7$ TeV. In this work, the Λ_b^0 decay is reconstructed in both, the signal $\Lambda_b^0 \to \Lambda^0\psi(2S)$ and the normalizing $\Lambda_b^0 \to \Lambda^0 J/\psi$ mode. The $\psi(2S)$ meson is reconstructed in the $\mu^+\mu^-$ decay channel, $J/\psi \to \mu^+\mu^-$ and Λ^0 decaying into $\mathrm{p}\pi^-$. In CMS the data are collected into

Table 5–1: 2011 Dataset and Luminosities

Dataset	L (pb^{-1})
/MuOnia/Run2011A-May10ReReco-v1/AOD	240.0
/MuOnia/Run2011A-PromptReco-v4/AOD	999.5
/MuOnia/Run2011A-05Aug2011-v1/AOD	437.3
/MuOnia/Run2011A-PromptReco-v6/AOD	721.7
/MuOnia/Run2011B-PromptReco-v1/AOD	2891.0

"primary datasets", "secondary datasets", and "central skims" for distribution to the computing resources. The Λ_b^0 sample, containing dimuons ($\mu^+\mu^-$) in the final state, was taken from the enriched dimuon skim "MuOnia" dataset (Table 5–1), where the Analysis Object Data - AOD a subset of RECOnstructed Data, containing only high-level objects which should be sufficient for most analysis and are smaller than RECO data. These group of datasets have similar characteristics, like experiment software release $CMSSW\_4\_2\_X$ ($CMSSW\_4\_2\_3$, $CMSSW\_4\_2\_4\_patch1$, $CMSSW\_4\_2\_8$, $CMSSW\_4\_2\_8\_patch3$, $CMSSW\_4\_2\_8\_patch6$ respectively), creation time, and the skim MuOnia that belongs to 2011 Primary Datasets for Physics. They were mixed together according to a certain luminosity value in order to get various signal with background samples.

The muons from the signal and from the normalization mode are required to match the same dimuon High Level Trigger (HLT), namely the displaced low dimuon mass trigger (LMT), in order to cancel out the trigger efficiency and the systematic uncertainties.

The triggers used in this analysis are shown in the Table 5–2.

Table 5–2: Low Mass Triggers (LMT) used in this work, with their main characteristics (the $*$ is LowMass_Displaced).

LMT name	$\|\eta\|$	$p_T^{\mu\mu}$	L_{xy}/σ	$cos(\alpha_{xy})$	$m(\mu\mu)$	p_T^{μ}	CL	DCA_{xy}
HLT_Dimuon6p5_*	<2.5	>6.5	>3	>0.9	1.0-5.0			
HLT_Dimuon7_*	<2.2	>6.9	>3	>0.9	1.0-4.8	>3.0	>5.0%	<0.5
HLT_DoubleMu4_*	<2.2	>6.9	>3	>0.9	1.0-4.8	>4.0	>15%	<0.5
HLT_DoubleMu4p5_*	<2.2	>6.9	>3	>0.9	1.0-4.8	>4.5	>15%	<0.5
HLT_DoubleMu5_*	<2.2	>6.9	>3	>0.9	1.0-4.8	>5.0	>15%	<0.5

Where the η is the pseudorapidity, p_T^{μ} and $p_T^{\mu\mu}$ are the muon and dimuon transverse momentum respectively (in GeV/c), L_{xy}/σ is the transverse separation between the dimuon vertex and the beamspot and σ is its uncertainty, $cos(\alpha_{xy})$ is the cosine of α which is the angle in the transverse plane between the dimuon momentum and the separation between the dimuon vertex and the beamspot, $m(\mu\mu)(GeV/c^2)$ is the dimuon invariant mass range, CL is the confidence level and finally the $DCA_{xy}(cm)$ is the Distance of Closest Approach between the dimuon momentum and the beamspot in the transverse plane.

The evolution of the LMT is very well described in the M. Dinardo Thecnical Report [31] and all the CMS B-Physics trigger in the Woehri, H web page [32].

In this study the analyzer uses Physics Analysis Toolkit (PAT) objects to extract and analyze the Λ_b^0 sample. PAT is a high-level analysis layer providing the Physics Analysis Groups (PAGs) with easy access to the algorithms developed by Physics Objects Groups (POGs) in the framework of the CMSSW offline software. PAT is fully integrated into CMSSW and an integral part of any release of CMSSW [33].

The CMSSW_4_2_8_patch7 software version was used in this work (CMSSW code is written in C++, which is maintained in a Concurrent Versions System (CVS) software repository. This version is the currently recommended analysis release for data and MC reconstructed with 4_2_X). Each run contains several luminosity sections, not all useful for the offline analysis, there are quite a lot of random triggers that occur when the detector is not taking data, and so to account for this, the best practice is to only run on luminosity sections where the detector was "on". Information on which luminosity sections in which runs are considered good and should be processed is collected in certification files that are in JSON format and are released weekly by the Certification Team. The good runs were selected with the "*MuonPhys*" JSON (Java Script Object Notation) file:

$$Cert\_160404 - 180252\_7TeV\_PromptReco\_Collisions11\_JSON\_MuonPhys.txt$$

Because of the complexity of High Energy Physics experiments and the impossibility of calculating every effect analytically, simulation methods are commonly used. Computers have pseudo-random number generators which are used to simulate approximations of expected results coming from the theoretical predictions. We call this simulation method Monte Carlo. Physics event generation and detector simulation are the earliest steps in the event processing chain that leads to producing a Monte Carlo sample. This involves several steps which pass generated physical processes through a simulation of the detector and allows physicists to see what new physics would look like when seen by the detector and hence where to concentrate their searches. An ample variety of the Monte Carlo samples for various types of physics analysis are produced and distributed centrally suitable for physics analysis [34]. (They can be found via Data Aggregation Service page [1]).

An official CMS Monte Carlo (MC) simulated signal event sample[2] is used to check the agreement with data, to tune the selection criteria, compute the acceptance and find the Λ_b^0 reconstruction efficiency. Table 5–3 shows the MC generated branching fraction[3] for these decays chain[4] from where we calculated the generated number of events for these two Λ_b^0 different modes. These numbers indicate the different decay likelyhood in this MC generated. The $B_{Gen}(J/\psi \to \mu^+\mu^-)$ in this table indicates that all the generated J/ψ particles are going to decay into two opposite charge muons, with the purpose of increase the production efficiency of

1 https://cmsweb.cern.ch/das/

2 /LambdaBToPsiMuMu_2MuPEtaFilter_Tight_7TeV-pythia6-evtgen/Fall11-HLTBPh2011_START42_V14B-v2/GEN-SIM-RECO

3 http://cmssw.cvs.cern.ch/cgi-bin/cmssw.cgi/CMSSW/GeneratorInterface/ExternalDecays/data/incl_BtoJpsi_mumu.dec

4 http://cmssw.cvs.cern.ch/cgi-bin/cmssw.cgi/CMSSW/GeneratorInterface/ExternalDecays/data/DECAY.DEC

the signal in our MC. In the same way, the others B_{Gen} values contribute to our MC generated (they do not need to be PDG standard values).

The total number of generated events were cross-checked by counting them directly from the MC Truth collection "genParticles", which is a Generator Particle Candidate [35] that brings the tools to match the reconstructed object to generated particle, it contains the generated four-momentum, charge, vertex, a PDG identifier and a status code in HepMC (an object oriented event record written in C++ for Monte Carlo Generators in High Energy Physics).

Table 5–3: Λ_b^0 MC generated branching fraction.

Decay Mode	MC generated branching fraction
$B_{Gen}(J/\psi \to \mu^+\mu^-)$	1
$B_{Gen}(\psi(2S) \to \mu^+\mu^-)$	0.1741
$B_{Gen}(\psi(2S) \to J/\psi\pi^+\pi^-)$	0.4762
$B_{Gen}(\Lambda_b^0 \to \Lambda^0 J/\psi)$	0.168
$B_{Gen}(\Lambda_b^0 \to \Lambda^0\psi(2S))$	0.053
$B_{Gen}(\Lambda^0 \to p\pi^-)$	0.6390

5.2 Event Selection

The strategy for physics analysis in CMS is based on the reconstruction of particles traveling through the detector components, which record the signal as it travels. This signal is reconstructed as individual points in space (recHits). The recHits are associated to form the particle trajectory, which leads to define the momentum, charge and the indentification of the particle.

Because this analysis was originally designed to search for $\Lambda_b^0 \to \Lambda^0\mu^+\mu^-$, events were selected without any particular $\mu^+\mu^-$ reconstructed invariant mass ($M_{\mu^+\mu^-}$) requirement. CMS has been designed and optimised to detect and reconstruct muons, and the input dataset is based on muon selection, however, the analysis strategy in this thesis consisted of first reconstructing the $\Lambda^0 \to p\pi^-$ then to look for an aditional muon pair ($\mu^+\mu^-$) originating from a common vertex. Once the Λ^0 and the $\mu^+\mu^-$ candidates are found, we reconstruct a "loose" [5] Λ_b^0 sample by computing its invariant mass and begin the analysis by examining the underlying $M_{\mu^+\mu^-}$ mass distribution in the sample.

In the process of taking a closer look into this distribution, the signal $\Lambda_b^0 \to \Lambda^0\psi(2S)$ has emerged naturally. At the same time to be able to reconstruct the well known Cabibbo Favoured $\Lambda_b^0 \to \Lambda^0 J/\psi$ decay (normalization mode), showing that all the tools needed for this analysis exist. The decay event topology of the cases $\Lambda_b^0 \to \Lambda^0\mu^+\mu^-$, $\Lambda_b^0 \to \Lambda^0\psi(2S)$ and $\Lambda_b^0 \to \Lambda^0 J/\psi$ are very similar and is sketched in Fig. 5–1. It consists, besides the particle identification, of finding two well displaced vertices, the $\mu^+\mu^-$ and the Λ^0, from the interaction point or beam spot.

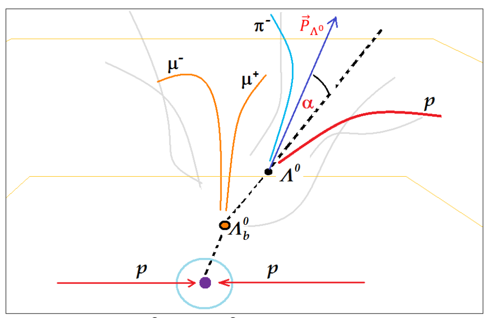

Figure 5–1: $\Lambda_b^0 \to \Lambda^0\mu^+\mu^-$ decay topology.

5.2.1 $\Lambda^0 \to p\pi^-$ Selection

The default reconstruction sequence in CMSSW includes a step that reconstruct neutral strange hadrons (K^0_{short} and Λ^0, collectively known as V0 particles) using oppositely charged track pairs [37]. The module for this reconstruction is called RecoVertex/V0Producer. This work began by selecting Λ^0 baryons from the experiment Vee collection ("*V0producer.generalV0Candidates*"). These candidates are reconstructed from two oppositely charged tracks with a common vertex displaced from the primary interaction. The tracks belong to a proton

[5] The cut severity levels are called: VeryLoose, Loose, Medium, Tight, SuperTight, HyperTight1, HyperTight2, HyperTight3, HyperTight4. The names would give an indication of how severe the cuts for the particle selection are [36].

and a pion ($\Lambda^0 \to p\pi^-$), where the hadron track with the highest p_t is identified as a proton, otherwise as a pion (this is because of the proton is more massive than pion).

The V0 reconstruction corresponds to the identification of the decay of a neutral particle to two opposite charged ones. The neutral particle does not produce a track in the experimental apparatus, while their daughter particles do. Therefore, the V0 reconstruction is performed searching for pair of tracks with opposite charge that satisfy certain geometrical criteria, i.e, that form a V shape topology, as illustrated in Fig. 5–2 [38].

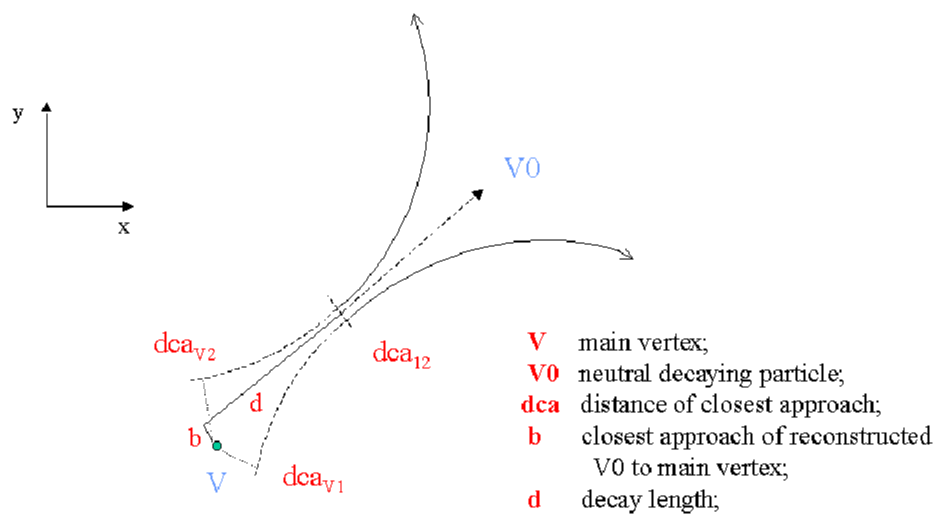

Figure 5–2: Schematic representation of a V0. The geometrical cuts used to identify it are: decay distance (d), impact parameter (b), distance of closest aproach of daughter tracks to primary vertex (dcaV1 and dcaV2) and distance of closest aproach between daughter tracks (dca12).

The number of reconstructed $\Lambda^0 \to p\pi^-$ (Fig. 5–5 -left) (size of the collection) per event in the MuOnia dataset input shows the number of Λ^0 candidates per event (multiplicity) from where the Λ_b^0 candidate sample is extracted . Due to the fact that the Λ^0 coming from Λ_b^0 have low momentum (because of the J/ψ momentum is bigger than the Λ^0 momentum, and its mass is bigger than the Λ^0 mass), the Λ^0 multiplicity has been enhanced with respect to the default vee collection since we have produced it with "*looser*" cuts on the Λ^0 two-dimensional (2-dim) vertex and impact parameter significance, where the significance is defined as the ratio of a measured quantity with respect to its uncertainty.

A loose cut of 5.0 (instead of default value of 15) has been required for the 2-dim vertex significance ("$vtxSignificance2DCut$") which is defined as the L_{xy}, which is displacement between the reconstructed Λ^0 vertex and the beamspot calculated in the transverse plane, divided by its standard deviation ($(L/\sigma)_{xy}$) Fig. 5–3.

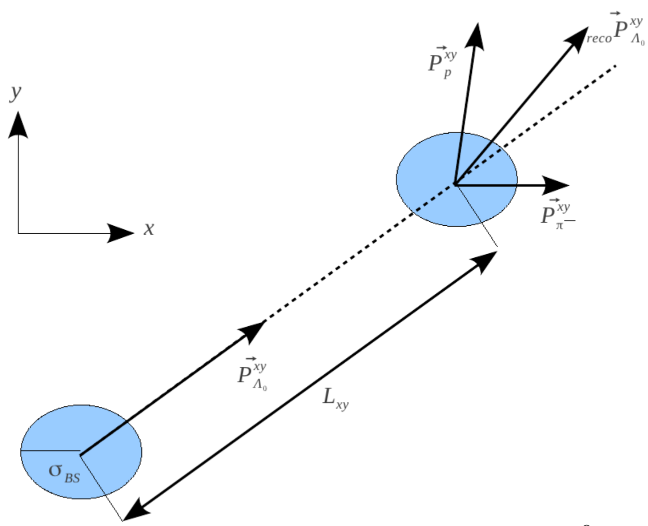

Figure 5–3: Scheme of the reconstructed Λ^0.

Another important selection cut is the distance between the primary vertex and the closest approach to the track, called the impact parameter (I_p). A visualization will help with understanding this (Fig. 5–4):

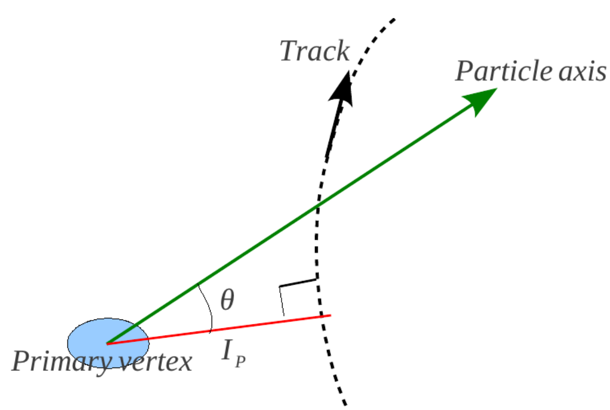

Figure 5–4: Visualization of the Impact Parameter (I_p, red line) of a track.

The track is represented by the dotted line. This track belongs to a particle (with a direction given by the green arrow). The Impact Parameter, is represented by the I_p line (red line), and is drawn from the primary vertex to the track. Notice how the point where the I_p touches the track, a right angle is formed, this is how the point of closest approach is identified. Also, the location where the I_p line makes a right angle with the track is unique. Meaning, the I_p always makes a right angle with the track, and there is only one I_p per track. However, the error on the I_p measurement could sometimes be large. To account for this we divided the I_p by its standard deviation, and this new value is called the I_p-Significance (Ip/σ_{Ip}). A "*loose*" cut of 0.5 (instead of 2) was required for the impact parameter significance ("*impactParameterSigCut*").

Table 5–4 shows a summary of these cuts as well as the default collection values.

Table 5–4: Loose $\Lambda^0 \to p\pi^-$ Selection Cuts.

Variable	Applied Cut	Default Cut
$(L/\sigma)_{xy}$	>5.0	>15
Ip/σ_{Ip}	>0.5	> 2

In addition, it is required to have a valid vertex kinematic fit and Λ^0 mass constraint fit to its nominal Λ^0 mass [39] in order to consider the Λ^0 a good candidate to then continue the search for the muon pair. A gaussian signal plus a linear polynomial fit on the pπ^- invariant mass on Fig. 5–5 -right shows that the "loose" Λ^0 candidate sample consists of approximately 24.3×10^6 $\Lambda^0 \to p\pi^-$ decays.

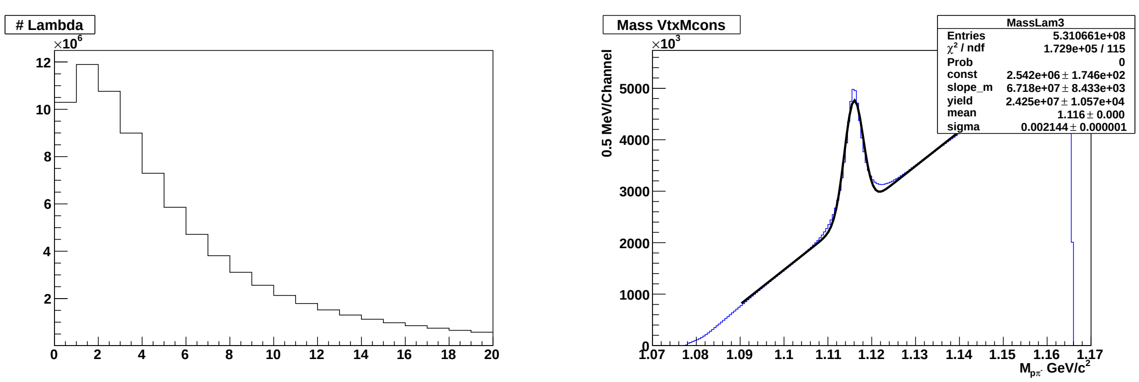

Figure 5–5: $\Lambda^0 \to p\pi^-$ multiplicity (left) and mass (right).

5.2.2 $\mu^+\mu^-$ Selection

PAT supports such a common frame of object disambiguation in a user configurable and well defined way. In the default configuration of the PAT workflow no objects are removed from the collections (i.e. cleanPatMuons), but overlapping objects from other collections, provides the opportunity to connect, for example, PAT objects with trigger objects for further studies. This association is provided by the TriggerMatching. A kind of this, is the "cleanPatMuonsTriggerMatch" collection in which, the muon's tracks are searched and reconstructed, once the "loose" Λ^0 candidate sample has been selected and events with two oppositely charged muons are chosen.

The reconstruction starts with the tracks in the muon detectors, called standalone muons. These tracks are then matched to tracks reconstructed in the silicon tracker (tracker muon), and the final muon objects are called global muons (G). These muons must satisfy the baseline POG muon tight cuts [40] show in Table 5–5, which consists of the following requirements, designed to suppress hadronic punch-throughs and muons from decays in flight [6] .

Table 5–5: Baseline muon selections.

1. recoMu.isGlobalMuon()
2. recoMu.globalTrack()$\rightarrow$ normalizedChi2() $<$ 10
3. recoMu.globalTrack()$\rightarrow$ hitPattern().numberOfValidMuonHits() $>$ 0
4. recoMu.numberOfMatchedStations() $>$ 1
5. recoMu.innerTrack()$\rightarrow$ hitPattern().numberOfValidPixelHits() $>$ 0
6. track()$\rightarrow$ hitPattern().trackerLayersWithMeasurement() $>$ 5

A brief description of each besaline muon selection is given below:

1. The muon candidate is reconstructed as a Global Muon

2. $\chi^2/ndof$ (ndof: number of degree of freedom) of the global-muon track. A global track is fitted using all hits belonging to the matching tracker and standalone tracks. If more than one global track is produced for a given standalone, the one with the best χ^2 is chosen [7] . For each standalone muon there is a maximum of one global muon that will be reconstructed [11].

[6] "Decays in Flight" vs "Punch-Through": for generated kaon and pion events, if there is a muon in the SIM collection we categorize the event as decay in flight, otherwise as punch-through [41].

[7] The z-coordinates of the points of closest approach of the tracks are referred to as z_i and the associated uncertainty is σ_i. The tracks must be assigned to some unknown number of vertices at positions z_k. The assigment probability of track i to vertex k is described by p_{ik}, having values between 0 and 1. The procedure then finds the most likely distribution of assigments for a given $<\chi^2>=\sum_{ik} p_{ik}\frac{(z_i-z_k)^2}{\sigma_i^2}$ referred to as the "principle of maximum entropy".

3. At least one muon chamber hit included in the global-muon track fit

4. Muon segments in at least two muon stations, this implies that the muon is also an arbitrated tracker muon - to suppress also and accidental track-to-segment matches. Also makes selection consistent with the logic of the muon trigger which requires segments in at least two muon stations to obtain a meaningful estimate of the muon p_T.

5. Number of pixel hits

6. Cut on number of tracker layers with hits >5 - to guarantee a good p_T measurement, for which some minimal number of measurement points in the tracker is needed.

Additionally, both of these muons must be inside of the pseudo-rapidity region where CMS muon reconstruction efficiency is high ($|\eta_\mu| < 2.2$). Neither of these muon tracks must be identified with any pion or proton tracks from Λ^0 found in the track collection "*cleanPatTrackCands*". Furthermore, it is also required the two muons to share a valid common vertex reconstructed within the volume of the CMS tracker, but significantly displaced from the LHC beam line.

The distance of closest approach is how close two charged particles can get to each other in a collision. The distance between the muons at their closest approach ($dca_{\mu^+\mu^-}$) is required to be less than 1 cm and their crossing point be inside the fiducial tracking volume. In order to suppress background from other heavier baryons decays ($\Xi^0 \to \Lambda^0\pi^0$, $\Sigma^0 \to \Lambda^0\gamma$, etc.) and to make sure the Λ^0 comes from the $\mu^+\mu^-$ vertex as expected, it is required that the cosine of the pointing angle (or pointing back angle α: is define as the angle between the vector connecting the primary and the secondary vertex and the reconstructed candidate momentum) between the p_T of Λ^0 and the $\mu^+\mu^-$- Λ^0 vertex direction (see Fig. 5–1) be above 0.95:

$$\cos\alpha_{\Lambda^0-\mu^+\mu^-} = \frac{(\vec{V}_{\mu^+\mu^-} - \vec{V}_{\Lambda^0}) \cdot \vec{P}_{\Lambda^0}}{|\vec{V}_{\mu^+\mu^-} - \vec{V}_{\Lambda^0}||\vec{P}_{\Lambda^0}|} > 0.95$$

in such a way the 3 body (Λ^0-$\mu^+\mu^-$) vertex coordinates can be approximated by the $\mu^+\mu^-$ vertex position.

5.2.3 Λ_b^0 Reconstruction

Finally, we take advantage of the event topology (Fig. 5–1) and kinematics of the long lived Λ_b^0 particle decays to determine additional requirements to reconstruct it. For instance, the reconstructed decay length and the Λ_b^0 trajectory pointing to the primary vertex ($\cos\alpha$) are two important variables which help in reducing unwanted prompt dimuon events.

The offline primary vertex reconstruction proceeds as follows:

• reconstructed tracks are selected based on their compatibilty with the beam spot, number of hits and fit quality

• the tracks are clustered into several primary vertex candidates, according to the z-coordinate of the point of closest approach of the tracks to the z-axis

• a (3d) vertex fit is performed with the tracks of each primary vertex candidate

• primary vertex candidates compatible with the beam line are retained [42].

In order to select the best primary vertex for this topology, in the "$offlinePrimaryVertices$" vertex collection, has to be search the closest vertex to the Λ_b^0 trajectory which is calculated by requiring that the cosine of the angle between the $\mu^+\mu^-$ Λ^0 total momentum ($\vec{P}_{\Lambda_b^0}$) and the primary:

$$\cos\alpha_{prim-\mu^+\mu^-} = \frac{(\vec{V}_{\mu^+\mu^-} - \vec{V}_{primary}) \cdot \vec{P}_{\Lambda_b^0}}{|\vec{V}_{\mu^+\mu^-} - \vec{V}_{primary}||\vec{P}_{\Lambda_b^0}|} > 0.95,$$

where the $\mu^+\mu^-$ vertex is the same as the Λ^0-$\mu^+\mu^-$ vertex as explained previously (Fig. 5–6).

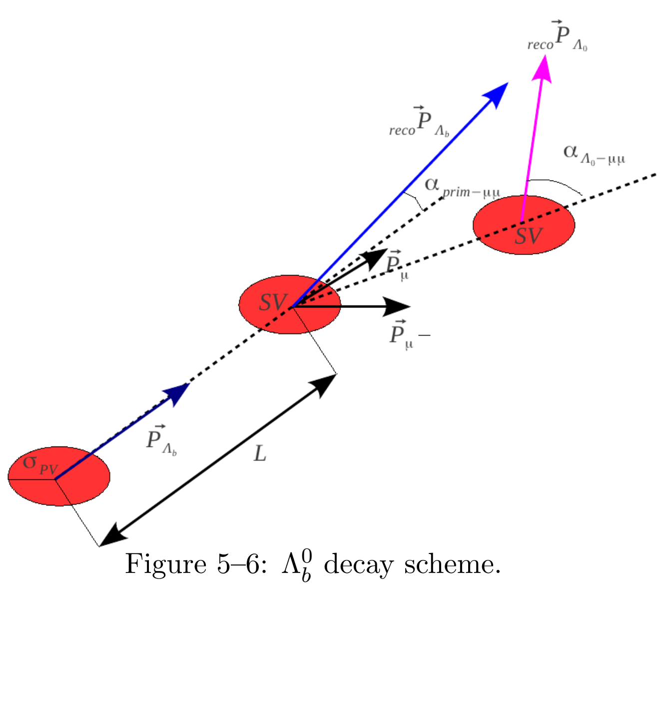

Figure 5–6: Λ_b^0 decay scheme.

The selected primary has been also refitted, excluding all the used tracks in the search, the two muons, the proton and the pion. To calculate the Λ_b^0 ("the Λ^0-$\mu^+\mu^-$ ") vertex detachment distance from the primary vertex, the decay length (L Fig. 5–6) is calculated and a minimun detachment by taking the decay length significance ($(L/\sigma)_{\Lambda_b^0}$) greater than 3 (Table 5–7) is required.

To clean even further the $\Lambda_b^0 \to \Lambda^0\mu^+\mu^-$ candidates sample, additional cuts have been applied to purify the Λ^0 (Table 5–6) and the $\mu^+\mu^-$ (Table 5–7) sample.

Table 5–6: $\Lambda^0 \to p\pi^-$ Selection Cuts

Variable	Applied Cut
$CL_{vtx}^{\Lambda^0 \to p\pi^-}$	>1%
$CL_{massC}^{\Lambda^0}$	>1%
$\lvert M_{p\pi^-} - M_{\Lambda^0}\rvert$	<10 MeV
$p_t^{\Lambda^0}$	>1.0 GeV
N_{hits}^{p}	>6
$N_{hits}^{\pi^-}$	>6
$\lvert M_{K_{short}^0} - M_{\pi^+\pi^-}\rvert$	>20 MeV

Table 5–7: $\mu^+\mu^-$ Selection and Λ_b^0 Reconstruction Cuts.

Variable	Applied Cut
$dca_{\mu^+\mu^-}$	<1 cm
$CL_{vtx}^{\mu^+\mu^-}$	>15%
both η_μ	<2.2
$(L/\sigma)_{\Lambda^0-\mu^+\mu^-}$	>3
$\cos\alpha_{\Lambda^0-\mu^+\mu^-}$	>0.95
$(L/\sigma)_{\Lambda_b^0}$	>3
$\cos\alpha_{prim-\mu^+\mu^-}$	>0.95
$p_t(\Lambda_b^0)$	>10 GeV

One of this cuts is called confidence level, which is a statistical method for setting upper limits on model parameters, a particular form of interval estimation used for parameters that can take only non-negative values. Interval in which is expected the true value of a given parameter. It was first introduced by physicists working at the LEP experiment at CERN and has since been used by many high energy physics experiments [43]. The probability for the confidence interval to contain (cover) a hypothesis parameter value is called the confidence level (CL). In this work, it is selected Λ^0 with quality cuts on the vertex confidence level for $p\pi^-$ ($CL_{vtx}^{\Lambda^0 \to p\pi^-}$), on the Λ^0 mass constraint fit ($CL_{massC}^{\Lambda^0}$) and on the reconstructed $p\pi^-$ invariant mass, which require to be 10 MeV around the nominal Λ^0 mass. In addition, to clean even further we requested that the p and π has a minimun number of tracking hits (6) and a minimum p_t for Λ^0 of 1.0 GeV to avoid proton mis-identification and to remove undesirable $K^0_{short} \to \pi^+\pi^-$ cross-feed contamination.

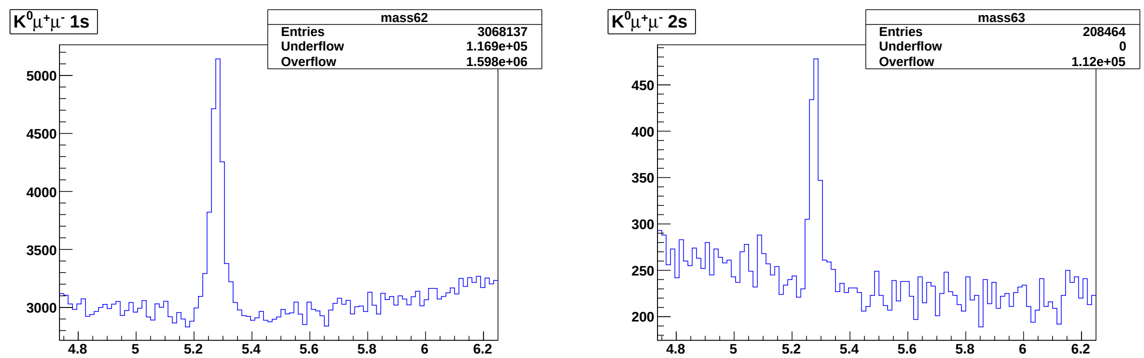

Figure 5–7: Invariant mass for K^0_{short} J/ψ (left) and K^0_{short} $\psi(2S)$ (right). A clear B^0 signal is observed which is removed after the Λ_b^0 cuts are applied.

To fully removed K^0_{short}, coming from $B^0 \to J/\psi K^0_{short}$ or $B^0 \to \psi(2s)K^0_{short}$ decays (Fig. 5–7), the 2-body invariant mass was re-calculated by changing the proton mass assignment for a pion and request that the $\pi^+\pi^-$ invariant mass be smaller than 20 MeV around the nominal K^0_{short} mass [39] to be tag as a K^0_{short} and then immediately rejected from this analysis.

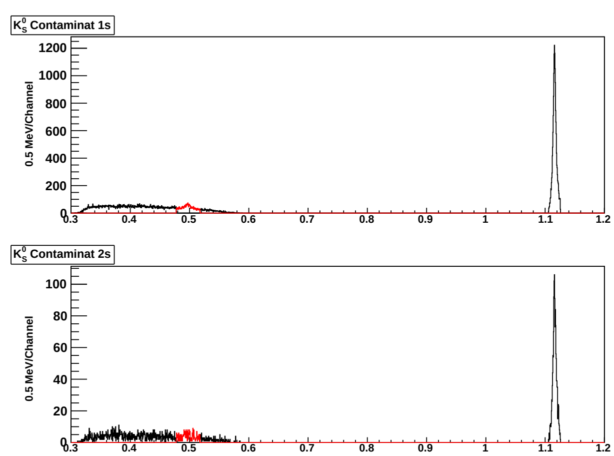

Figure 5–8: $p\pi^-$ (graphics right side) and $\pi^+\pi^-$ (graphics left side) invariant masses for the Λ^0 J/ψ sample (top graphic) and Λ^0 $\psi(2S)$ sample (botton graphic). The Λ^0 on the right is kept while the K^0_{short} contamination ($|M_{K^0_{short}} - M_{\pi^+\pi^-}|$<20 MeV) is removed in the final Λ_b^0 sample.

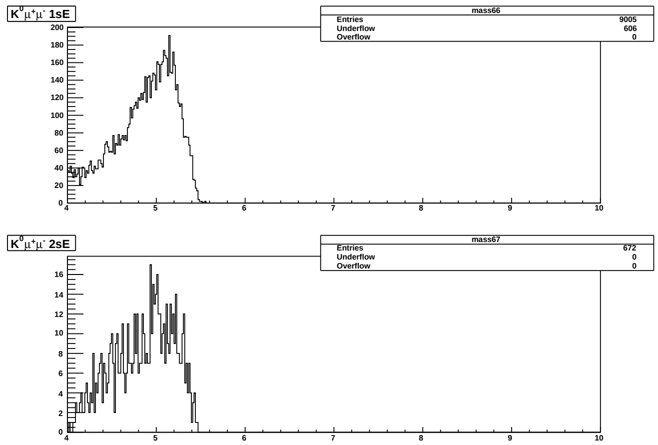

Figure 5–9: B^0 signal underneath the Λ_b^0 candidate.

Fig. 5–8 shows the $K^0_{short} \to \pi^+\pi^-$ contamination ($|M_{K^0_{short}} - M_{\pi^+\pi^-}| < 20\ MeV$) in the J/$\psi$ (left side in the upper plot) and in the $\psi(2S)$ (left side in the botton plot) modes which has been removed (red part) from the Λ_b^0 candidate sample while the right side shows the $\Lambda^0 \to p\pi^-$ kept for the Λ_b^0 sample. Fig. 5–9 shows the remaining negligible B^0 candidates underneath the final Λ_b^0 samples peak. This contamination is not included in the signal MC we are using, so we search for Λ_b^0 decay in an enriched B^0 MC dataset [8] . In this sample we have applied all the Λ_b^0 base line cuts (Table 5–5, Table 5–7, and good pπ^- vertex), but the Λ^0 quality cuts (Table 5–6). The reconstructed $B^0 \to J/\psi K^0_{short}$ and $B^0 \to \psi(2s)K^0_{short}$ are shown in Fig. 5–10, Now adding all the Λ^0 cuts including K^0_{short} veto, we obtained that this cross-feed is negligible, despite Λ_b^0 and B^0 have a similar topology (Fig. 5–11).

In order to remove combinatorial background, it is requested that the separation significance ($(L/\sigma)_{\Lambda^0-\mu^+\mu^-}$) between Λ^0 and $\mu^+\mu^-$ to be greater than 3 to make sure they are coming from two well separated different vertices. A summary of these cuts are shown in Table 5–6 for Λ^0 and Table 5–7 for the $\mu^+\mu^-$ selection cuts as well as the cuts to select Λ_b^0 candidates (lower part in Table 5–7). In addition a kinematic cut on the Λ_b^0 transverse momentum ($p_t(\Lambda_b^0) > 10\ GeV$) has been applied in order to reduce the remaining combinatorial background. Adding all the cuts described in Tables 5–6 and 5–7 including the K^0_{short} veto, we

[8] /B0ToPsiMuMu_2MuPEtaFilter_Tight_7TeV-pythia6-evtgen/Fall11-HLTBPh2011_START42_V14B-v2/GEN-SIM-RECO

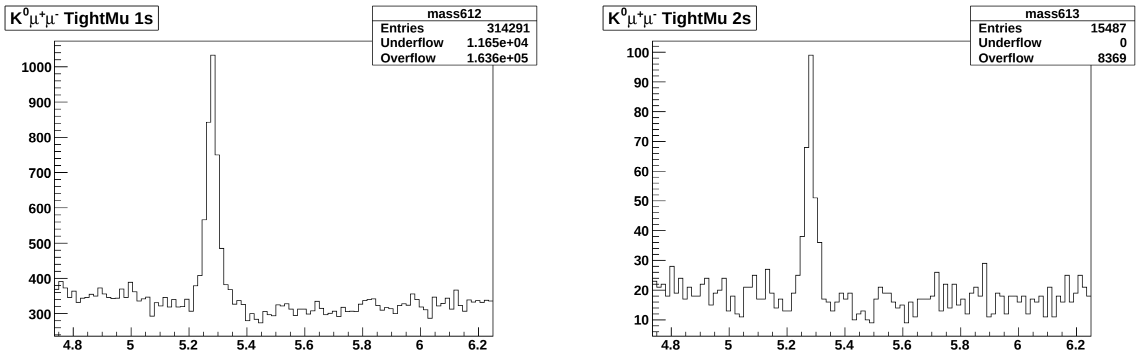

Figure 5–10: Invariant mass for K^0_{short} J/ψ (left) and K^0_{short} $\psi(2S)$ (right). A clear B^0 signal is observed in the MC sample.

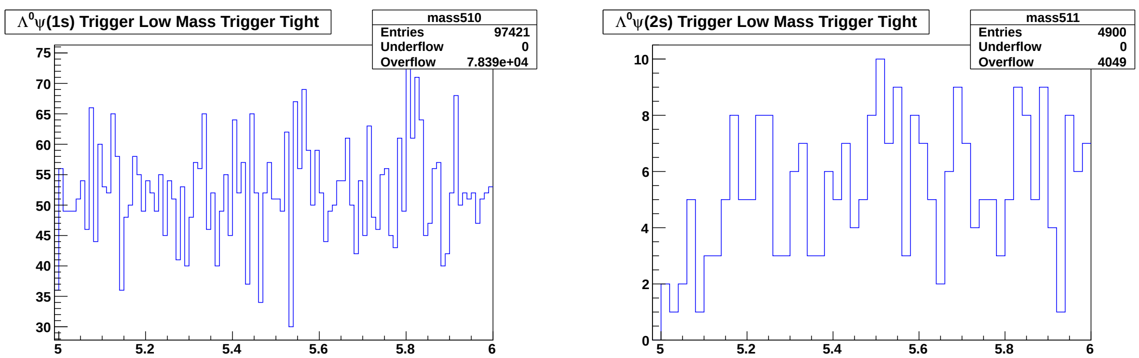

Figure 5–11: Invariant mass for Λ^0 J/ψ (left) and Λ^0 $\psi(2S)$ (right). There is not Λ_b^0 signal in the B^0 MC sample, the crossfeed is negligible.

obtain a clear Λ_b^0 peak at its nominal mass of 5.620 GeV [39]. Fig. 5–12 shows the Λ^0 $\mu^+\mu^-$ invariant mass, which is the sample from where we look for associate production of $\mu^+\mu^-$ together with Λ^0 particles.

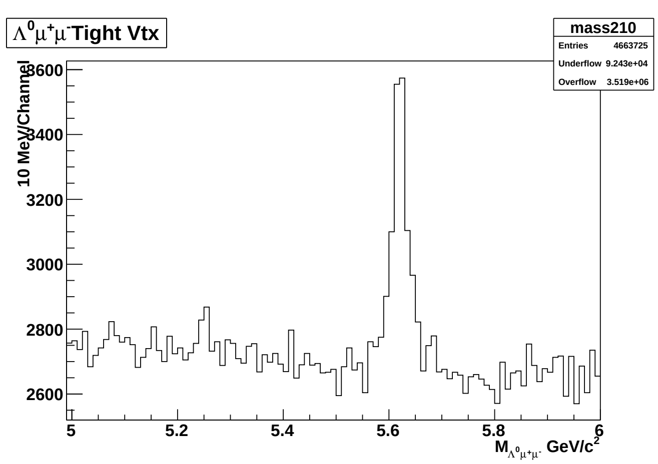

Figure 5–12: Λ^0 $\mu^+\mu^-$ Invariant mass for 2011.

5.3 Data Analysis

The study of the $\Lambda_b^0 \to \Lambda^0\psi(2S)$ decay began by investigating the underlying dimuon invariant mass distribution in the $\Lambda_b^0 \to \Lambda^0\mu^+\mu^-$ candidate sample (Fig. 5–12). We have noticed, by calculating the mass difference ($M_{\Lambda^0\mu^+\mu^-} - M_{\mu^+\mu^-}$) and the dimuon mass $M_{\mu^+\mu^-}$, that the main contribution to the Λ_b^0 sample are the charmonium states J/ψ and $\psi(2S)$ as expected from the cabibbo expectator diagram shown in Fig. 3–2. The top distribution in Fig. 5–13 shows the mass difference $M_{\Lambda^0\mu^+\mu^-} - M_{\mu^+\mu^-}$ for reconstructed $\mu^+\mu^-$ masses in the range of 2.9 $< M_{\mu^+\mu^-}$ <3.8 GeV, where the sharp peak around 2.5 GeV is the well known $\Lambda_b^0 \to \Lambda^0 J/\psi$ decay. To find an evidence of the $\Lambda_b^0 \to \Lambda^0\psi(2S)$ decay, we just look the dimuon mass distribution (Fig. 5–13 - bottom) under the Λ_b^0 resonance (5.620 GeV $\pm$ 0.05 GeV) which shows a J/ψ and $\psi(2S)$ mesons decaying into $\mu^+\mu^-$ as a clear evidence of the Λ_b^0 decay into Λ^0 $\psi(2S)$.

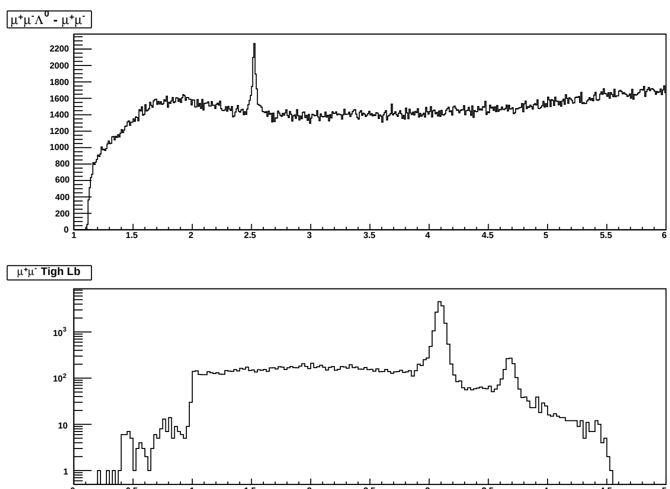

Figure 5–13: $M_{\Lambda^0\mu^+\mu^-} - M_{\mu^+\mu^-}$ (top) and $M_{\mu^+\mu^-}$ (bottom) Invariant Mass.

Next, the mass constrained fit is applied to the measured $\mu^+\mu^-$ system to improve the dimuon momentum resolution and consequently the Λ_b^0 mass resolution. They were fitted by constraining their measured invariant mass to their nominal values [39] if the $M_{\mu^+\mu^-}$ fall within 150 MeV around the J/ψ or the $\psi(2S)$ reconstructed mass. The confidence level of the fit is required to be better than 1%, otherwise the $\mu^+\mu^-$ combination is rejected.

5.3.1 $\Lambda_b^0 \to \Lambda^0\psi(2S)$ with $\psi(2S) \to \mu^+\mu^-$

The event topology of these decays (Fig. 5–14) is very similar with the one sketched in Fig. 5–1 with the only difference that in this case the $\mu^+\mu^-$ comes from one of the charmonium states (J/ψ or $\psi(2S)$), which have equivalent topologies. In addition, because the recorded $\psi(2S)$ event sample in the $\mu^+\mu^-$ decay mode satisfied the LMT, we required that the normalization J/ψ mode also satisfy the same trigger in order to cancel out the systematic effects.

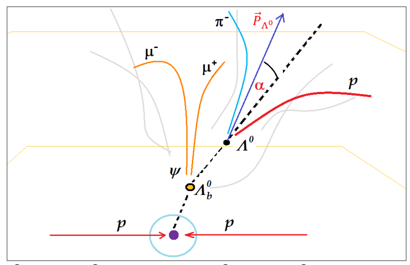

Figure 5–14: $\Lambda_b^0 \to \Lambda^0 J/\psi$ or $\Lambda_b^0 \to \Lambda^0\psi(2S)$ decay topology.

To reduce the HLT trigger rate, the trigger was taken with a variable muon p_t threshold as the instantaneous luminosity increased [31]. In this analysis, a straight cut on the muon transverse momentum of 4.5 GeV (instead of change it with time) and a $\mu^+\mu^-$ momentum cut of 6.9 GeV was applied in order to match the LMT conditions since the other requirements for the trigger (Table 5–7) were already applied. Table 5–8 summarized the additional cuts to extract these exclusive decays as well as to match the LMT.

Table 5–8: Extra cuts and LMT matching cuts.

Variable	Applied Cut
$\lvert M_{J/\psi} - M_{\mu^+\mu^-}\rvert$	<150 MeV
$\lvert M_{\psi(2S)} - M_{\mu^+\mu^-}\rvert$	<150 MeV
CL_{massC}	>1%
p_t muon	>4.5 GeV
$P_T^{\mu^+\mu^-}$	>6.9 GeV

Finally, the Λ_b^0 invariant mass was computed by combining the mass fitted Λ^0 and $\mu^+\mu^-$ four-momentum, this combination is fitted with a gaussian function to describe the signal peak and a linear function for the background (Fig. 5–15).

At the same time, to calculate the relative Λ_b^0 reconstruction efficiency, the MC sample was analyzed and treated under the same conditions as data, including the HLT. The number of signal (S) events obtained in the fit for data and for Λ_b^0 Monte Carlo signal is reported in Table 5–9 (and in Fig. 5–15). The fitted mass and the standard deviation for the $\Lambda_b^0 \to \Lambda^0\psi(2S)$ are 5.623 ±0.003 GeV and 17.7 ±3.0 MeV respectively. Significance is introduced to quantify the probability of a statistical fluctuation to observed S events or more when you expect only B events (background). A significance estimator is $S/\sqrt{B}$ (for large S) [44], which for this signal is 7.8 σ.

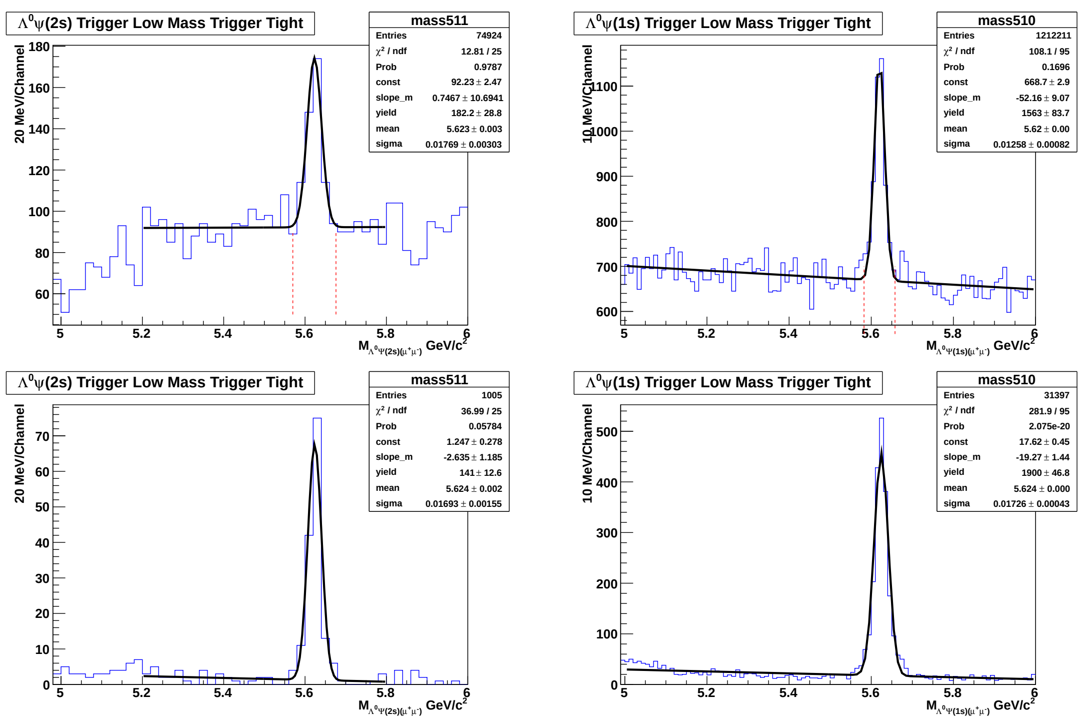

Figure 5–15: Λ^0 $\psi(2S)$ (left) and Λ^0 J/ψ (right) Mass. Top(data) and Bottom(mc).

Table 5–9: Number of Events in the $\psi(2S) \to \mu^+\mu^-$ Mode

(displaced low dimuon mass trigger (LMT))

Decay Mode	S (Events)	Signif	$S_{MC}(Events)$
$\Lambda_b^0 \to \Lambda^0\psi(2S)$	182.19 ±28.80	7.8 σ	141.03 ±12.60
$\Lambda_b^0 \to \Lambda^0 J/\psi$	1563.06 ±83.73	21.2σ	1900.33 ±46.75

5.3.2 Λ_b^0 Branching Ratio Measurements

The absolute branching fraction of a decay is the fraction of produced particles which decay by an individual decay mode with respect to the total number of decaying particles [24], in this case:

$$B(\Lambda_b^0 \to \Lambda^0\psi(2S)) = \frac{N^{prod}_{\Lambda_b^0\to\Lambda^0\psi(2S)}}{N^{Total}_{\Lambda_b^0\to\Lambda^0\psi(2S)}},$$

where N^{Total} is the total number of particles which in this case corresponds to the luminosity $\mathscr{L}$ of the experiment, and $N^{prod}_{\Lambda_b^0\to\Lambda^0\psi(2S)}$ is the number of produced Λ_b^0 particles which is related to the number of observed particles (reconstructed) by the reconstruction efficiency, as follows:

$$N^{prod}_{\Lambda_b^0\to\Lambda^0\psi(2S)} = \frac{N^{rec}_{\Lambda_b^0\to\Lambda^0\psi(2S)}}{\epsilon^{rec}_{\Lambda_b^0\to\Lambda^0\psi(2S)}}$$

The efficiency is obtained from a MC run and can be written as:

$$\begin{aligned}\epsilon^{rec}_{\Lambda_b^0\to\Lambda^0\psi(2S)} &= \frac{N^{rec}_{\Lambda_b^0\to\Lambda^0\psi(2S)}}{N^{Gen}_{\Lambda_b^0\to\Lambda^0\psi(2S)}} * \frac{N^{trig}_{\Lambda_b^0\to\Lambda^0\psi(2S)}}{N^{rec}_{\Lambda_b^0\to\Lambda^0\psi(2S)}} \\ &= \epsilon^{rec} * \epsilon^{trigger}\end{aligned}$$

where ϵ^{rec} is the reconstruction efficiency, which included the geometrical acceptance and all the selection cuts, and $\epsilon^{trigger}$ is the number of the reconstructed Λ_b^0 particles which satisfied the HLT trigger (LMT).

Now, replacing the previous equations and taking into account the Λ_b^0 decaying to $\Lambda^0 \to p\pi^-$ and $\psi(2S) \to \mu^+\mu^-$, the absolute branching fraction for the $\Lambda_b^0 \to \Lambda^0\psi(2S)$ is:

$$B(\Lambda_b^0 \to \Lambda^0\psi(2S)) * B(\psi(2S) \to \mu^+\mu^-) * B(\Lambda^0 \to p\pi^-) = \frac{N^{rec}_{\Lambda_b^0\to\Lambda^0\psi(2S)}}{\epsilon^{rec} * \epsilon^{trigger} * \mathscr{L}}$$

where we have included the term $B(\psi(2S) \to \mu^+\mu^-) * B(\Lambda^0 \to p\pi^-)$ which represent the branching fraction for $\psi(2S) \to \mu^+\mu^-$ and $\Lambda^0 \to p\pi^-$,

$$B(\Lambda_b^0 \to \Lambda^0\psi(2S)) = \frac{N^{rec}_{\Lambda_b^0\to\Lambda^0\psi(2S)}}{\epsilon^{rec} * \epsilon^{trigger} * \mathscr{L} * B(\psi(2S) \to \mu^+\mu^-) * B(\Lambda^0 \to p\pi^-)} \tag{5.1}$$

Similarly, the absolute branching fraction for the $\Lambda_b^0 \to \Lambda^0 J/\psi$ is given by:

$$B(\Lambda_b^0 \to \Lambda^0 J/\psi) = \frac{N_{\Lambda_b^0 \to \Lambda^0 J/\psi}}{\epsilon^{rec} * \epsilon^{trigger} * \mathscr{L} * B(J/\psi \to \mu^+\mu^-) * B(\Lambda^0 \to p\pi^-)}, \tag{5.2}$$

where $\mathrm{N}_{\Lambda_b^0 \to \Lambda^0 J/\psi}$ is the number of $\Lambda_b^0 \to \Lambda^0 J/\psi$ signal events reconstructed in data and equivalently (with Eq. (5.1)) the other terms but in this case for $\Lambda_b^0 \to \Lambda^0 J/\psi$.

Taking advantage of the similar topology of these modes, it is very convenient to measure the unknown signal branching fraction $\mathrm{B}(\Lambda_b^0 \to \Lambda^0 \psi(2S))$ with respect to the known $\mathrm{B}(\Lambda_b^0 \to \Lambda^0 J/\psi)$ in such a way that the integrated luminosity and the trigger efficiency cancel out when both samples comes from the same dataset input (as this analysis) and both samples satisfy exactly the same trigger. To make sure that this ratio is one, we plot the reconstructed MC Λ_b^0 in both modes (Fig. 5–16) ($\psi(2S)$ and J/ψ) before the LMT conditions are applied, then dividing the yields from these figures by their corresponding MC after the trigger cuts (Fig. 5–15), we obtained the relative trigger efficiency:

$$(\epsilon_{\Lambda_b^0 \to \Lambda^0 J/\psi}/\epsilon_{\Lambda_b^0 \to \Lambda^0 \psi(2S)})^{trigger} = 0.99 \pm 0.10(stat)$$

which then cancels out as expected.

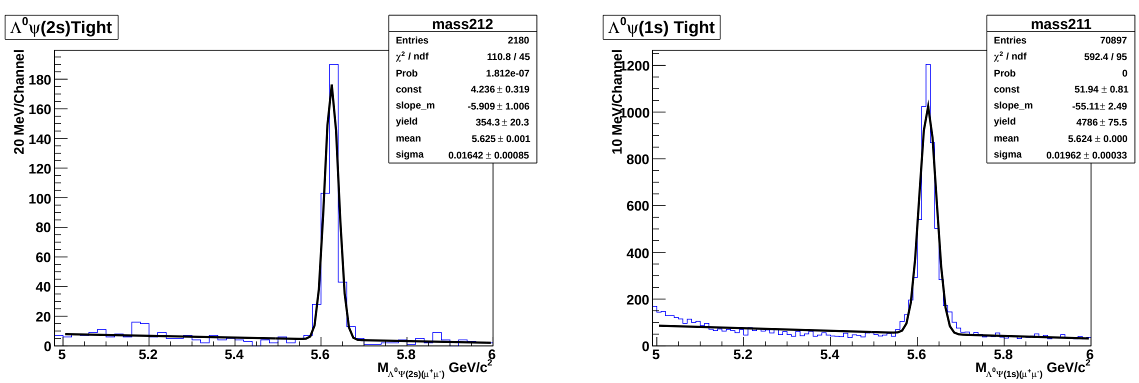

Figure 5–16: MC Λ_b^0 reconstructed sample

Thus, dividing equation (5.1) by equation (5.2) and canceling $\mathscr{L}$, $\epsilon^{trigger}$ and $\mathrm{B}(\Lambda^0 \to p\pi^-)$, the relative branching fraction formula is:

$$\frac{B(\Lambda_b^0 \to \Lambda^0 \psi(2S))}{B(\Lambda_b^0 \to \Lambda^0 J/\psi)} = \frac{N_{\Lambda_b^0 \to \Lambda^0 \psi(2S)}}{N_{\Lambda_b^0 \to \Lambda^0 J/\psi}} \left(\frac{\epsilon_{\Lambda_b^0 \to \Lambda^0 J/\psi}}{\epsilon_{\Lambda_b^0 \to \Lambda^0 \psi(2S)}} \right)^{rec} * f_c, \tag{5.3}$$

with branching fraction factor

$$f_c = \frac{B(J/\psi \to \mu^+\mu^-)}{B(\psi(2S) \to X)},$$

which in the case of $\psi(2S) \to \mu^+\mu^-$, B($\psi(2S)$ →X) ≡ B($\psi(2S) \to \mu^+\mu^-$), f_c is:

$$f_c = \frac{B(J/\psi \to \mu^+\mu^-)}{B(\psi(2S) \to \mu^+\mu^-)} = \frac{5.93\% \pm 0.06\%}{0.77\% \pm 0.08\%} = 7.7013 \pm 0.8039(stat). \tag{5.4}$$

Now, we used the MC sample to measure the relative Λ_b^0 reconstruction efficiency:

$$\left(\frac{\epsilon_{\Lambda_b^0 \to \Lambda^0 J/\psi}}{\epsilon_{\Lambda_b^0 \to \Lambda^0 \psi(2S)}}\right)^{rec} = \left(\frac{N_{\Lambda_b^0 \to \Lambda^0 J/\psi}}{N_{\Lambda_b^0 \to \Lambda^0 \psi(2S)}}\right)^{MCrec} * f_{gen} \tag{5.5}$$

where the generated MC factor is defined as:

$$f_{gen} = \left(\frac{N_{\Lambda_b^0 \to \Lambda^0 \psi(2S)}}{N_{\Lambda_b^0 \to \Lambda^0 J/\psi}}\right)^{Gen}.$$

The number of generated events are counted by using the MC generated branching fraction from Table 5–3. In the case of the $\psi(2S) \to \mu^+\mu^-$, the MC gen factor is:

$$f_{gen} = \frac{B_{Gen}(\Lambda_b^0 \to \Lambda^0 \psi(2S))}{B_{Gen}(\Lambda_b^0 \to \Lambda^0 J/\psi)} * \frac{B_{Gen}(\psi(2S) \to \mu^+\mu^-)}{B_{Gen}(J/\psi \to \mu^+\mu^-)} = \frac{0.053}{0.168} * \frac{0.1741}{1} = 0.055 \tag{5.6}$$

Replacing the relative reconstruction efficiency (equation 5.5) in the relative branching fraction (equation 5.3), the final expression:

$$\frac{B(\Lambda_b^0 \to \Lambda^0 \psi(2S))}{B(\Lambda_b^0 \to \Lambda^0 J/\psi)} = \left(\frac{N_{\Lambda_b^0 \to \Lambda^0 \psi(2S)}}{N_{\Lambda_b^0 \to \Lambda^0 J/\psi}}\right) * \left(\frac{N_{\Lambda_b^0 \to \Lambda^0 J/\psi}}{N_{\Lambda_b^0 \to \Lambda^0 \psi(2S)}}\right)^{MC} * f_{gen} * f_c. \tag{5.7}$$

Measurement B($\Lambda_b^0 \to \Lambda^0 \psi(2S)$) with $\psi(2S) \to \mu^+\mu^-$

In order to measure the relative branching fraction, the yields from Table 5–9 are replaced in formula (5.7):

$$\frac{B(\Lambda_b^0 \to \Lambda^0 \psi(2S))}{B(\Lambda_b^0 \to \Lambda^0 J/\psi)} = \left[\frac{182.19 \pm 28.80}{1563.06 \pm 83.73}\right] * \left[\frac{1900.33 \pm 46.75}{141.03 \pm 12.60}\right] * 0.055 * (7.7013 \pm 0.8039),$$

where the factors f_{gen} and f_c were taken from equation (5.6) and (5.4). Calculating, we obtained a preliminary measurement in this mode:

$$\frac{B(\Lambda_b^0 \to \Lambda^0 \psi(2S))}{B(\Lambda_b^0 \to \Lambda^0 J/\psi)} = 0.66 \pm 0.11(stat) \pm 0.07(syst) \pm 0.07(PDG)$$

where the first term is the statistical uncertainty [9] , the last term is the uncertainty from the ratio $B(\psi(2S) \to \mu^+\mu^-)/B(J/\psi \to \mu^+\mu^-)$ taken from the PDG [39] and the systematic uncertainties included (syst) only the biases due to offline event selection/cuts and are described in the next section. This result is still under the review process by the CMS collaboration.

5.3.3 $\Lambda_b^0 \to \Lambda^0\psi(2S)$ Systematic Uncertainties

These systematic uncertainties on the branching fraction are based on loosing and tightening the baseline cuts (Table 5–6, Table 5–7 and 5–5) used to extract the Λ_b^0 signal. The method used here was to change some cuts like $\cos\alpha_{prim-\mu^+\mu^-}$, $p_t(\Lambda_b^0)$, muonId and the fitted function to the Λ_b^0 signal, which in this case was a polynomial of degree 2 for background, plus a gaussian function for signal, and see how the branching fraction central value ($Br_{cv} = 0.66$) changes with respect to these parameters, with the formula: $\dfrac{Br_{cv} - Br_n}{Br_{cv}} * 100$. The value Br_n is obtained when the parameter n is change.

A summary of the source of systematic uncertainties are listed in Table 5–10 and shown in Fig. 5–17. These were combined (Total) using a root sum-of-the-squares approach (in quadrature) to give an estimate for the total relative uncertainty on the branching fraction.

Table 5–10: Systematic Uncertainties

Source	Cut	Variation wrt central value (%)
Tightening $\cos\alpha_{prim-\mu^+\mu^-}$	>0.99	2.66%
Loosing $p_t(\Lambda_b^0)$	>5	1.24%
Loosing muonId Tight cuts	Only at least 1 G	9.57%
Background shape	P2 + Gauss	0.43%
Total		10.02%

The total systematic uncertainty is 10.02%, which is multiplied by the relative branching fraction central value (0.66) to obtaine the 0.07 (syst) value. The most significant contribution comes from loosing muonId Tight cuts, however, this measurement has a little bit better statistical error and was considered in the total systematic. If this is not taken into account then

[9] The satistical uncertainties were combined using quadrature: $\sigma = x * y * z * \sqrt{(\frac{\Delta x}{x})^2 + (\frac{\Delta y}{y})^2 + (\frac{\Delta z}{z})^2}$

the systematic is very small. The bottom first point in Fig. 5–17 represents the central value for the branching fraction while the rest are the systematics for this mesurement.

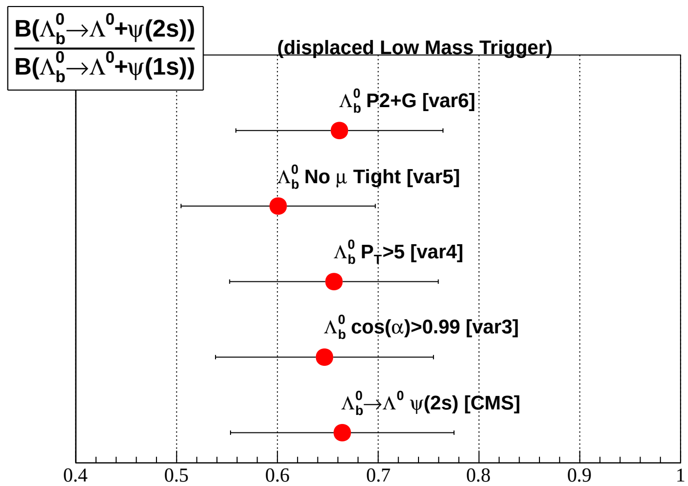

Figure 5–17: Relative Branching Ratio for $\Lambda_b^0 \to \Lambda^0\psi(2S)$

Chapter 6
CONCLUSIONS

Based on the 2011 data with 5.3 fb^{-1} of luminosity, collected by the CMS experiment in pp collisions at centre of mass energy of 7 TeV at the LHC, the $\Lambda_b^0 \to \Lambda^0 \psi(2S)$ decay mode has been observed for the first time, where the final state has been reconstructed in $\psi(2S) \to \mu^+\mu^-$ and Λ^0 in the $p\pi^-$ final states.

The branching fraction for the $\Lambda_b^0 \to \Lambda^0 \psi(2S)$ signal has been measured with respect to the most copious charmonium Λ_b^0 decay ($\Lambda_b^0 \to \Lambda^0 J/\psi$). A preliminary measurement of the relative branching fraction led to:

$$\frac{B(\Lambda_b^0 \to \Lambda^0 \psi(2S))}{B(\Lambda_b^0 \to \Lambda^0 J/\psi)} = 0.66 \pm 0.11(stat) \pm 0.07(syst) \pm 0.07(PDG)$$

where the normalizing mode Λ^0 J/ψ has been reconstructed with $J/\psi \to \mu^+\mu^-$. Because both of these states have the same topology, the systematic uncertainties and the trigger efficiency cancel out. This preliminary measurement is still under review by the CMS collaboration and it does not represent an official result in anyway.

It is important to note that our data show a clear signal around the nominal Λ_b^0 invariant mass value, but the background underneath is considerably higher than the expected, probably because our first analysis approximation was to point the Λ^0 particle to the dimuon vertex instead of doing the two objects (dimuon-Λ^0) vertex constraint. In order to improve the signal to noise (background) ratio of this result, we are working on tuning the selection criteria to reduce the background, for example the selection criteria related with the proton and pion identification, vertex constraints, etc.

As the statistical uncertainty is the largest in this measurement, is statistically dominated and can be improved by increasing the input data. One way is including another $\psi(2S)$ decay mode, as $\psi(2S) \to J/\psi\pi^+\pi^-$, in the analysis, while another way is analyzing more data. The group already started working with dataset from the 2012 proton run which consist of approximately 20 fb^{-1} of luminosity collected by the experiment at the centre of mass energy of 8 TeV.

To avoid Λ^0 mis-identification due to the similar decay topology to our signal, an enriched $B^0 \to K_s^0\psi(2S)$ signal MC data was studied to look for our decay $\Lambda_b^0 \to \Lambda^0\psi(2S)$. The reconstructed MC B^0 invariant mass spectrum shows that the contamination or cross-feed from this decay is negligible and does not affect to the main result.

Even though our study is on b-quark barions, we noticed that our relative branching fraction follows the same trends as many b-quark meson (B) branching ratios decaying into charmonium final states, as for instance the branching fraction for B^+ decays taken from the PDG table [39] gives:

$$\frac{B(B^+ \to K^+\psi(2S))}{B(B^+ \to K^+J/\psi)} = 0.65 \pm 0.05$$

Fig. 6–1 shows six of these B mesons decaying into charmonium states ($\psi(2S)$ +X)/(J/ψ +X) where X represents a π^+, K^0_{short}, Λ^0, etc., where the bottom point is our preliminary measurement.

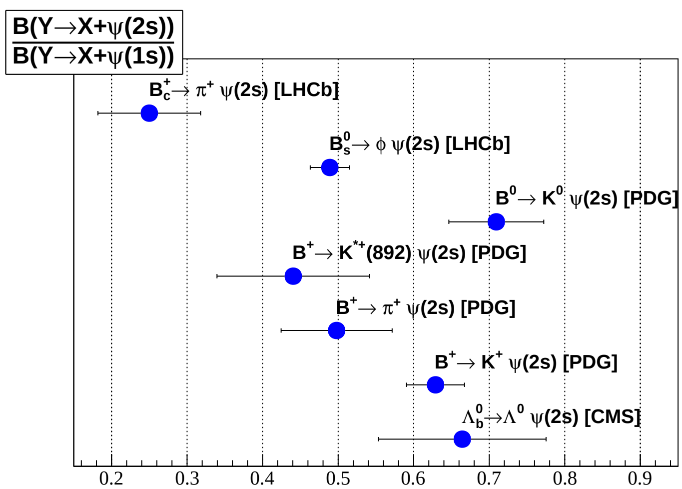

Figure 6–1: Relative branching fraction for b baryons (CMS) and meson (PDG).

Bibliography

[1] A. D. Martin F. Halzen. *"Quarks and Leptons: An Introductory Course in Modern Particle Physics"*. Institute of Physics Publishing, Bristol and Philadelphia, second edition, 2002.

[2] AJG Hey IJR Aitchison. *"Gauge Theories in Particle Physics", Volume I: From Relativistic Quantum Mechanics to QED*. Institute of Physics Publishing, Bristol and Philadelphia, third edition, 2002.

[3] J. Allday. *"Quarks, Leptons and the Big Bang"*. Institute of Physics Publishing Bristol and Philadelphia, second edition, 2002.

[4] A. Korytov. "Data Analysis Basics". www.phys.ufl.edu/~korytov/phz6355/note_A13_statistics.pdf.

[5] H. R. Quinn R. M. Bernet. *"The Charm of Strange Quarks, Mysteries and revolutions of particle physics"*. Springer-Verlag, second edition, 2000.

[6] The CMS Collaboration. "Search for the standard model Higgs boson produced in association with a top-quark pair in pp collisions at the LHC". *Submitted to J. High Energy Phys.*

[7] CMS Collaboration. "Observation of a new boson with mass near 125 GeV in pp collisions at $\sqrt{s} = 7\ TeV$ and $8\ TeV$". *Submitted to Eur. Phys. J. C*, 31 Mar 2013.

[8] B. R. Martin. *"Nuclear and Particle Physics: An Introduction"*. John Wiley and Sons, first edition, 2006.

[9] D. A. Greenwood W. N. Cottingham. *"An Introduction on the Standard Model of Particles Physics"*. Cambridge University Press, second edition, 2007.

[10] CERN 2013. "The LHC experiments". http://public.web.cern.ch/PUBLIC/en/LHC/LHCExperiments-en.html.

[11] D. Fasanella. *"Study of the X(3872) state with the CMS experiment at LHC"*. Thesis University de Bologna, 2012.

[12] CERN Press Office (17 December 2012). "The first LHC protons run ends with new milestone". http://press.web.cern.ch/press-releases/2012/12/first-lhc-protons-run-ends-new-milestones.

[13] A. Pierce G. Kane. *"Perspectives on LHC PHYSIC"*. University of Michigan, USA, World Scientific, 4th edition, 2008.

[14] R. Cid Manzano X. Cid Vidal. "PHYSICS AT LHC". http://www.lhc-closer.es.

[15] CMS Collaboration. "LHC machine". *JINST*, 3 S08001, 2008.

[16] CMS Collaboration. "CMS physics technical design report volume 1: Detector performance and software". Technical report, 2006.

[17] CMS Collaboration. "Technical Proposal for the Upgrade of the CMS Detector Through 2020, Technical Design Report". Technical report, 2011.

[18] S. Fiorendi. *"Study of the $B_c \to J/\psi\pi$ and $B \to J/\psi K$ decay channels in the CMS experiment at LHC"*. Thesis, University Degli Studi Di Milano - BICOCCA, 2010-2011.

[19] Wikipedia. "Software framework". http://en.wikipedia.org/wiki/Software_framework.

[20] TWiki. "More on CMSSW Framework ". https://twiki.cern.ch/twiki/bin/view/CMSPublic/WorkBookMoreOnCMSSWFramework.

[21] TWiki. "Data Formats and Data Tiers". https://twiki.cern.ch/twiki/bin/view/CMSPublic/WorkBookDataFormats#EvenT.

[22] TWiki. "CMSSW Application Framework ". https://twiki.cern.ch/twiki/bin/view/CMSPublic/WorkBookCMSSWFramework.

[23] Fermilab. "Fermilab experiment discovers a heavy relative of the neutron". http://phys.org/news/2011-07-fermilab-heavy-relative-neutron.html.

[24] D. Griffiths. *"Introduction to Elementary Particles"*. John Wiley Sons, Inc, 1987.

[25] Wikipedia. " Lambda baryon ". http://en.wikipedia.org/wiki/Lambda_baryon#cite_note-PDGBottomLambda0-7.

[26] D0 Collaboration. "Measurement of the production fraction times branching fraction $f(b \to \Lambda_b^0)(\Lambda_b^0/\psi\Lambda)$". *Phys. Rev. D. 84, pages 031102 1-031102 7*, 2011.

[27] UA1 Collaboration. "First observation of the beauty baryon Λ_b^0 in the decay channel $\Lambda_b^0 \to \Lambda^0 J/\psi$ at the CERN proton-antiproton collider".

[28] N. Cabibbo. "Unitary Symmetry and Leptonic Decays". *Phys. Rev. Lett. 10, 531*, 1963.

[29] T. Maskawa M. Kobayashi. *"CP Violation in the Renormalizable Theory of Weak Interactions"*. Prog. Theor. Phys. 49, 652, 1973.

[30] CMS Collaboration (S. Chatrchyan *et al.*). "Observation of a New Ξ_b Baryon". *Phys. Rev. Lett.*, 108:252002, Jun 2012.

[31] M. Dinardo *et al.* "Angular Analysis and differential branching fraction of the decay $B^0 \to K^{*0}\mu^+\mu^-$". CMS Internal Note 2012/119, 2012. http://cms.cern.ch:80/iCMS/analysisadmin/get?analysis=BPH-11-009-pas-v0.pdf.

[32] H. Woehri. "Evolution of Muon Trigger Menu 03/05/2011". https://espace.cern.ch/cms-quarkonia/trigger-bph/default.aspx.

[33] Twiki. " Physics Analysis Toolkit (PAT) ". https://twiki.cern.ch/twiki/bin/view/CMSPublic/WorkBookPAT.

[34] Twiki. " Thirty Seconds Introduction to Generation and Simulation ". https://twiki.cern.ch/twiki/bin/view/CMSPublic/WorkBookGenIntro.

[35] Twiki. " Generator event format in AOD ". https://twiki.cern.ch/twiki/bin/view/CMSPublic/WorkBookGenParticleCandidate.

[36] Twiki. "Cuts in Categories" (CiC) Electron Identification". https://twiki.cern.ch/twiki/bin/view/CMSPublic/SWGuideCategoryBasedElectronID#Data_and_MC_optimization.

[37] Twiki. "V0Producer Offline Guide". https://twiki.cern.ch/twiki/bin/view/CMSPublic/SWGuideV0Producer.

[38] M. Munhoz. " Strangeness Reconstruction - Cuts Optimization ". http://www4.rcf.bnl.gov/~munhoz/strange/neural_net.html.

[39] Particle Data Group J. Beringer *et al.* "The Review of Particle Physics". *Phys. Rev. D*, 86:010001, 2012.

[40] MuonPOG. "Baseline muon selections". https://twiki.cern.ch/twiki/bin/view/CMSPublic/SWGuideMuonId#Tight_Muon.

[41] A. Everett *et al.* "Muon Identification in CMS". *CMS AN-2008/0988*, 2008.

[42] Twiki. "Offline Primary Vertex Production ". https://twiki.cern.ch/twiki/bin/view/CMSPublic/SWGuideOfflinePrimaryVertexProduction.

[43] J. Conrad (CERN). "Confidence Intervals in Particle (Astro-) physics". http://www.physik.unizh.ch/seminars/tpseminar/abstract_ws2k5/Zurich_30112005.pdf.

[44] A. Korytov. "Data Analysis Basics". www.phys.ufl.edu/~korytov/phz6355/note_A13_statistics.pdf.